Karson, J.A., Cannat, M., Miller, D.J., and Elthon, D. (Eds.), 1997
Proceedings of the Ocean Drilling Program, Scientific Results, Vol. 153

3. SERPENTINIZATION AND HYDROTHERMAL VEINING IN PERIDOTITES AT SITE 920 IN THE MARK AREA[1]

Yildirim Dilek,[2] Angela Coulton,[3] and Stephen D. Hurst[4]

ABSTRACT

Cores from Site 920 in the Mid-Atlantic Ridge at the Kane Transform (MARK) area record polyphase deformation in two holes reaching 126 and 200 m depth in serpentinized peridotites with minor metagabbros, amphibolite gneiss, and diabase units. The majority of the recovered mantle-derived rocks are composed of serpentinized harzburgites, which display a variably elongated, medium- to coarse-grained porphyroclastic texture produced by high-temperature crystal-plastic deformation. The porphyroclastic texture is overprinted by an anastomosing foliation defined by dark green to black serpentine and magnetite bands that wrap around orthopyroxene porphyroclasts. These bands are composed of a variant of mesh-textured serpentine, and contain mainly lizardite ± chrysotile, whereas mesh centers consist of fine-grained lizardite + brucite. Serpentine fibers in the bands are generally wall perpendicular, suggesting that the foliation is mainly a dilational fabric. The anastomosing foliation is cut by a set of veins (V1), which contain serpentine + actinolite ± chlorite ± talc and oblique-slip fibers. They display a wide range of dips with no preferred dip orientation, and indicate shearing synchronous with dilation. Compared to veins of later generations and to the pseudomorphic serpentine, serpentine in the V1 veins is relatively rich in iron, with FeO (total Fe as FeO) content ranging from 4.55 to 5.76 wt%. A network of thin and discontinuous veins (V2) composed of chrysotile and magnetite postdates the V1 veins and is either parallel to the anastomosing foliation and to the mesoscopic porphyroclastic fabric or, less commonly, is at a high angle to the foliation. Both the intensity of the anastomosing foliation and the spacing and distribution of V2 veins are strongly dependent on the porphyroclast content of the peridotite; a reduction in the pyroxene content commonly coincides with a drop in the intensity of the anastomosing foliation and the near absence of V2 veins. The V2 veins have a mean attitude of 336°/29°NE for both holes that overlaps with the corrected attitudes of the anastomosing foliation and the mesoscopic porphyroclastic fabric. More discrete and commonly branching veins (V3) crosscut the V2 veins and contain pale green-white chalky serpentine identified as lizardite, with minor amounts of carbonate and clay minerals, pyrite, and magnetite. They display wall-parallel bands with a pseudofibrous internal fabric and wallrock inclusions characteristic of antitaxial crack-seal veins. They have consistently steep dips in both holes. The latest generation (V4) of veins contains carbonate, pyrite, and/or clay minerals, and locally reactivates the earlier veins.

The dominant fabric of the anastomosing foliation and the serpentine mineral phases in serpentinized peridotites indicates that much of the hydration and static serpentinization occurred at temperatures around 350°–400°C. Gabbroic veins and veinlets represent a phase of magmatic veining in the serpentinized peridotites before formation of the hydrothermal veins, and they are altered by Ca-enriched fluids under greenschist facies conditions at temperatures of 300°–400°C. The V1 veins with oblique slip-fibers indicate dilation and contemporaneous shearing that enhanced fluid circulation into the serpentinized peridotites under greenschist facies conditions. The V2 veins are mainly extensional, as evidenced by the wall-perpendicular serpentine fibers. They were produced by elevated pore fluid pressures contemporaneous with stress release during exhumation of the peridotites. Reactivation of these veins during later extensional events and the generation of V3 crack-seal veins were related to further unroofing of the serpentinites and their emplacement along the rift valley walls because of extensional tectonics. Composite V4 veins containing carbonate + pyrite ± clay minerals indicate the sealing of extensional fractures in the serpentinized peridotites and the cessation of fluid flow following the emplacement of the ultramafic suite on the western wall of the median valley. Structural evidence from the core samples studied and the regional geological data suggest that the exposure of serpentinized peridotite on the seafloor in the MARK area is a result of exhumation by tectonic extension in the absence of an active magma chamber, rather than a result of diapiric ascent of serpentinite.

INTRODUCTION

The occurrence of serpentinized peridotites on the median valley walls of the Mid-Atlantic Ridge indicates that seafloor spreading processes and accretion of oceanic lithosphere along this slow-spreading ridge system have involved significant attenuation of the lower crust and uplift and exhumation of upper mantle at and near the spreading axis (Michael and Bonatti, 1985; Karson et al., 1987; Rona et al., 1987; Mével et al., 1991; Cannat et al., 1992). Emplacement of mantle-derived rocks at shallow crustal depths and on the seafloor is interpreted to have resulted from a complex interplay of mechanical extension and magmatic construction (Karson and Dick, 1983; Rona et al., 1987; Karson, 1990; Cannat, 1993; Cannat et al., 1995). Detailed studies of these rocks are thus anticipated to provide significant information on the magmatic, metamorphic, and tectonic processes attending seafloor spreading.

The Mid-Atlantic Ridge at the Kane Transform (MARK) area and its immediate environs have been the focus of numerous geophysical and bathymetric surveys and have been sampled extensively by dredging, submersible, and two Ocean Drilling Program (ODP) studies (Legs 109 and 153; for an extensive bibliography on previous studies in the MARK area, see Cannat, Karson, Miller, et al., 1995). During Leg 109, Site 670 was drilled in the serpentinized peridotites situated on the western rift valley about 35 km south of the Kane Transform (Fig. 1; Detrick et al., 1990). Various types of partially to completely serpentinized harzburgites were recovered during Leg

[1]Karson, J.A., Cannat, M., Miller, D.J., and Elthon, D. (Eds.), 1997. *Proc. ODP, Sci. Results,* 153: College Station, TX (Ocean Drilling Program).

[2]Department of Geology and Geography, Vassar College, Poughkeepsie, NY 12601, U.S.A. Present address: Department of Geology, Miami University, Oxford, OH 45056, U.S.A. dileky@muohio.edu

[3]Department of Geosciences, State University of New York at Albany, Albany, NY 12222, U.S.A.

[4]Department of Geology, Duke University, Durham, NC 27708, U.S.A.

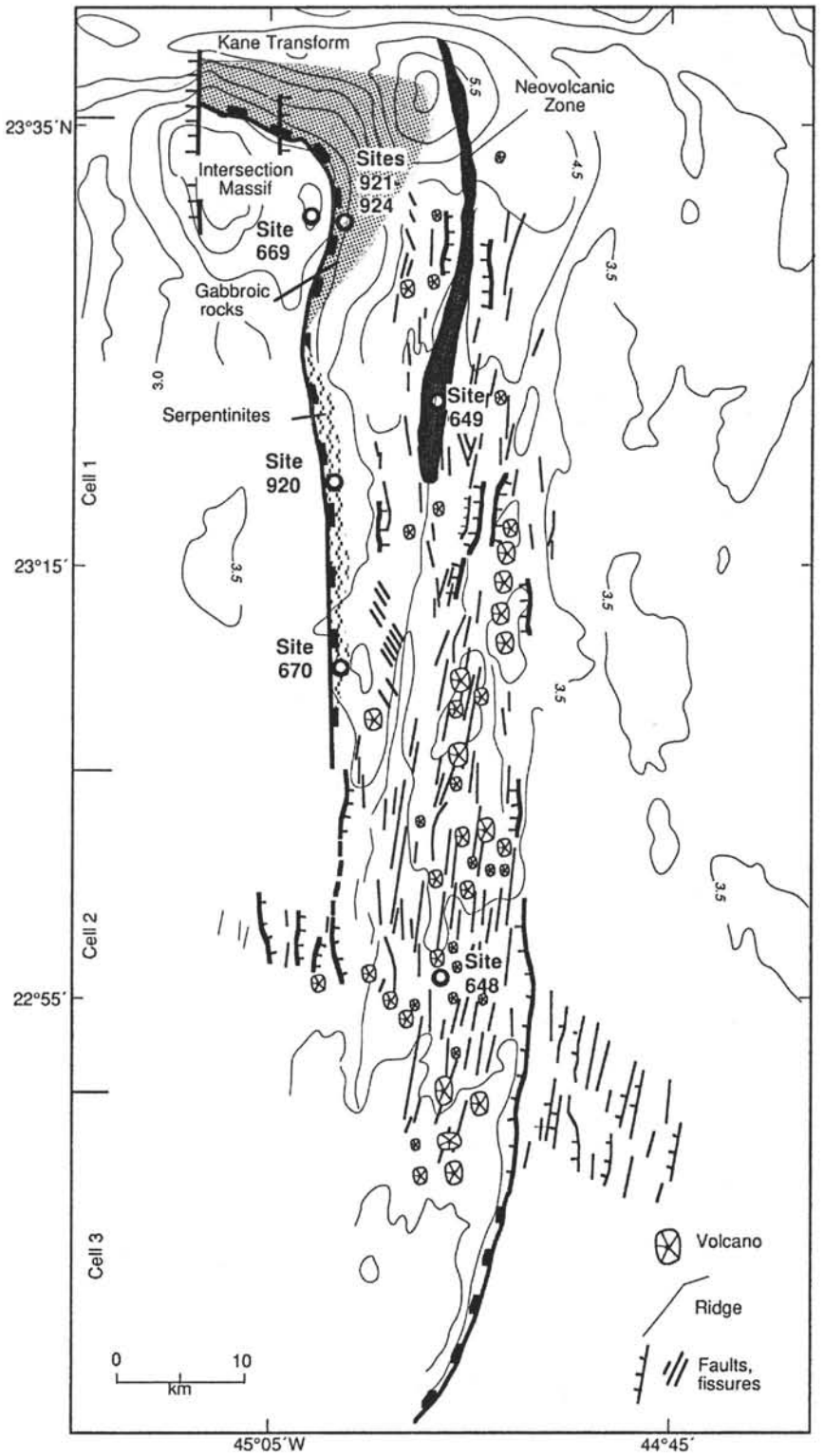

Figure 1. General bathymetric map of the MARK area showing simplified geology and ODP sites (open circles). Shading marks area of gabbroic rock outcrops; zigzag pattern represents area of serpentinized peridotite outcrops.

109 at Site 670 (Cannat et al., 1990; Hébert et al., 1990; Juteau et al., 1990). In 1994, Site 920 was drilled nearly 18 km north of Site 670 (Fig. 1). It recovered serpentinized ultramafic rocks that consist mainly of massive harzburgite with local interlayers of pyroxene-rich (up to 35% orthopyroxene) and pyroxene-poor harzburgite to dunite (Shipboard Scientific Party, 1995). Holes 920B and 920D reached depths in excess of 126 and 200 m, respectively, and recovered a total of 150 m of serpentinized harzburgite with several horizons of variably deformed and metamorphosed mafic rocks. These rocks record complex histories involving multiple deformational episodes, melt injection, strain localization, and successive episodes of serpentinization and hydrothermal veining of mantle-derived rocks during their uplift and emplacement on the ocean floor.

In this study, we document the nature and relative timing of bulk-rock serpentinization and hydrothermal vein development at Site 920 through structural and petrological analyses of serpentinized peridotites and hydrothermal vein generations hosted in these ultramafic rocks. A particular focus is placed on the documentation of hydro-

thermal veins, vein mineralogy and chemistry, and crosscutting relationships of different veins in variously serpentinized peridotites sampled from the core. New paleomagnetic data (Hurst et al., this volume) are used to reorient the planar fabric elements and different vein types in the geographic coordinate system to interpret their geometry and orientation in the tectonic framework of the MARK area. Findings of this study are then used to construct an approximate temperature-time-deformation path for upper mantle peridotites at temperatures below 500°C in a slow-spreading ridge system, as exemplified by the MARK area.

GEOLOGICAL OVERVIEW OF SITE 920

The MARK area is located just south of the Kane Transform on the Mid-Atlantic Ridge at about 23° N latitude and encompasses two spreading cells, a northern cell extending from the northern nodal basin to 23°18′N and a southern cell beginning south of 23°05′N (Fig. 1). These two spreading cells are separated by a broad discordant zone interpreted as a zero-offset transform fault (Purdy and Detrick, 1986). The northern cell appears to be a ridge segment in which tectonic extension has been dominant until a very recent magmatic event (Karson, 1990). The axial rift valley in this cell is characterized by a continuous median valley ridge, which narrows and deepens as the ridge-transform intersection is approached. The median valley is markedly asymmetrical; the western wall is substantially steeper and higher than the eastern wall. Photographic traverses and observations from the *Alvin* and *Nautile* show that the western wall contains a diverse assemblage of variably deformed and metamorphosed basaltic, gabbroic, and ultramafic rocks (Karson and Dick, 1983; Karson et al., 1987; Brown and Karson, 1988; Mével et al., 1991). These lithologies occur in high-angle fault blocks in the hanging wall of an undulating, low-angle detachment surface or a series of subparallel faults (Fig. 1).

Site 920 is located on a gently sloping terrace at the top of a steep cliff exposing massive to schistose, serpentinized peridotite on the western wall nearly 30 km south of the Kane Transform (Fig. 1). The terrace lies at a depth of 3340 meters below sea level (mbsl), and is covered with a smooth blanket of pelagic ooze and an unknown thickness of poorly consolidated rubble (Shipboard Scientific Party, 1995). The serpentinized peridotite outcrop extends nearly continuously from about 3500 mbsl to about 3100 mbsl and is cut by east-facing normal? faults. Faults with relatively steep dips (40°–70°) cut a more pervasive, gently east-dipping (20°–40°) schistosity, which is interpreted to be related to earlier, low-angle faults and shear zones (Karson et al., 1987; Mével et al., 1991).

The predominant rock types recovered from Site 920 include serpentinized harzburgite, with lesser amounts of lherzolite, dunite, clinopyroxenite, and websterite, along with variably altered olivine gabbro, gabbro, oxide-rich gabbroic rocks, amphibolitized microgabbro, amphibolite, rodingitized gabbro, and plagioclase-olivine phyric diabase (Shipboard Scientific Party, 1995). Porphyroclastic harzburgites display heterogeneous alteration, with the most intense alteration (95–100%) occurring in orthopyroxene-poor zones, and they locally contain 2- to 20- wide mylonitic zones. Some of these mylonitic zones are spatially associated with metagabbroic intervals in the core and contain highly deformed and recrystallized ultramafic and gabbroic material (i.e., Samples 153-920D-2R-1, 116–119 cm; 2R-1, 138–141 cm), which underwent extensive grain-size reduction of primary phases.

Amphibolites and amphibolitized microgabbro intervals are recovered from both Holes 920B and 920D. The amphibolite interval in Hole 920B (Sample 153-920B-13R-4, Piece 3) contains linear mafic aggregations of neoblastic brown amphibole and porphyroclasts of olivine, clinopyroxene, and magnetite forming fine-grained anastomosing bands, which are bounded by segregations of neoblastic plagioclase (Shipboard Scientific Party, 1995). This texture defines a moderately developed foliation and a well-developed lineation, and indicates formation at transitional granulite to amphibolite facies conditions. The amphibolite is juxtaposed against a gneissic metagabbro along a vertical contact in the core that is composed of alternating lenses of elongate plagioclase augen, fine-grained plagioclase neoblasts, and magnetite-rich stringers in an anastomosing foliation. The contact is subparallel to the foliation both in the gneissic metagabbro and amphibolite and is accompanied by a narrow magnetite- and ilmenite-rich ribbon. The gneissic metagabbro displays a porphyroclastic texture defined by coarse-grained, elongated plagioclase porphyroclasts that show sutured grain boundaries and extensive subgrain development. Orthopyroxene porphyroclasts are enclosed in a fine-grained matrix consisting of recrystallized plagioclase neoblasts, amphibole, and clay minerals.

Pyroxenite and gabbroic veins occur as millimeter- to centimeter-scale intervals in the serpentinized peridotites and crosscut the background mesh-textured serpentine in the host rock. They are commonly pervasively altered, and the primary phases are replaced by hydrous calcium-aluminum silicates (Shipboard Scientific Party, 1995). Clinopyroxene in gabbroic veins is altered to brown amphibole, actinolite, chlorite, secondary clinopyroxene, pyrite, and magnetite, whereas plagioclase is replaced by secondary plagioclase, prehnite, epidote, zoisite, chlorite, actinolite, and zeolite minerals (Shipboard Scientific Party, 1995). These secondary mineral assemblages and associated textural relations record static metamorphism of gabbroic veins under greenschist to zeolite facies conditions, and suggest that these magmatic intrusions have undergone incipient rodingitization.

Moderately olivine + plagioclase phyric diabases recovered from both Holes 920B and 920D represent 1.5-m- to 3.3-m-thick, tabular intrusive bodies in the serpentinized peridotites (Shipboard Scientific Party, 1995). The diabasic rock has a porphyritic intergranular to subophitic texture with euhedral olivine and tabular plagioclase phenocrysts, and is moderately to highly altered. Alteration mineral assemblages (i.e., chlorite, tremolite-actinolite, secondary plagioclase, epidote, prehnite, clay minerals) suggest metamorphism under greenschist to zeolite facies conditions (Shipboard Scientific Party, 1995).

ANALYTICAL METHODS

Forty-five samples of serpentinized peridotite selected from Holes 920B and 920D were examined in this study. Petrographic observations of thin sections were used to establish textural relationships and vein crosscutting relationships, and to identify preliminary mineral phases. The terminology used to describe serpentine textures is adopted from Wicks and Whittaker (1977). Serpentine minerals were formally identified by powder X-ray diffraction. The samples were gently ground in an agate pestle and mortar and were loaded in a glass sample holder for analysis. They were scanned from 8° to 64° 2θ at 2° per min on a Scintag diffractometer, equipped with a solid-state detector, using Cu Kα radiation at 40 kV and 45 mA. Quantitative analysis was carried out by the Rietveld refinement technique. This method is a whole-pattern-fitting, least squares technique that uses the entire pattern rather than a limited number of reflections to extract the required information. In this method, the observed pattern for each phase is compared with the calculated one (modeled using single-crystal structural data), and any differences between the two are minimized by least squares calculation. This involves optimizing both structural and profile-related parameters. Complex mixtures with phases containing overlapping reflections are quantified with a high degree of accuracy (1–2 wt%). The technique does not require any external "pure" standards. Reinterpretation of the X-ray diffraction analyses was done using diffraction data for Lizardite 1T, lizardite 6T, chrysotile 2Mcl, and chrysotile 2Orcl, found in Wicks and O'Hanley (1988). Although X-ray diffraction analyses give information on the dominant serpentine mineral present, it can be extremely difficult to identify small amounts of other serpentine minerals within a mixture. Although the mineralogy of textural intergrowths on a millimeter-scale can be resolved using microbeam X-ray diffraction

methods (Wicks and Zussman, 1975), serpentine group minerals may be intergrown on a micron scale. The best technique for analyzing serpentine mineralogy may therefore be high-resolution transmission electron microscopy (HRTEM) because the structural differences between lizardite, antigorite, and chrysotile allow clear identification at this scale.

Electron microprobe analyses aided the identification of fine-grained minerals associated with rodingitized gabbro veinlets and opaque minerals within the serpentinites. Electron microprobe analyses of various serpentine phases and chlorite were obtained using a JEOL Superprobe at Rensselaer Polytechnic Institute. Operating conditions were as follows: accelerating voltage = 15 kV, beam current = 25 nA, and beam diameter = 10 μm. Counting times were 5 s for Si and Mg and 30 s for all other elements. It is important to note that chemical compositions of serpentine minerals determined by electron microprobe analyses should be considered approximate because ocean-floor serpentinization commonly involves micron-scale intergrowths of serpentine-group minerals, chlorite, and brucite as well as metastable phases.

STRUCTURE AND PETROLOGY OF WHOLE-ROCK SERPENTINIZATION AND HYDROTHERMAL VEINING

Ultramafic lithologies recovered at Site 920 are extensively altered and are affected by at least 75% replacement of primary minerals, with most intervals displaying 85%–100% alteration (Shipboard Scientific Party, 1995). They are characterized by extensive development of mesh-textured serpentine, with minor amounts of talc, amphibole, and chlorite. The widespread alteration is associated with multiple generations of microscopic to mesoscopic, magmatic, and hydrothermal veins (Table 1). Magmatic veins include centimeter-scale pyroxenitic and gabbroic melt intrusions and commonly display wallrock reaction zones. Some of these magmatic veins were reactivated during later hydrothermal episodes involving brittle deformation.

Whole-Rock Serpentinization and the Anastomosing Serpentine Fabric

The pervasive background alteration of the peridotites at Site 920 is associated with an anastomosing foliation overprinting a mesoscopic porphyroclastic fabric (Ceuleneer and Cannat, this volume), which was previously interpreted as a crystal-plastic fabric (Shipboard Scientific Party, 1995). The mesoscopic porphyroclastic fabric is composed of an early crystal-plastic fabric overprinted by an anastomosing serpentine fabric, and is defined by subparallel alignment of variably elongated porphyroclasts containing aggregates of orthopyroxene, olivine, and clinopyroxene. The crystal-plastic fabric represents mantle flow planes that are defined by the preferred orientation of olivine grains and by the elongation of individual spinel and/or orthopyroxene grains (Ceuleneer and Cannat, this volume). Pyroxene porphyroclasts are wrapped by a subparallel network of composite, generally less than 1 mm-wide, serpentine and serpentine + magnetite bands producing the anastomosing foliation (Fig. 2). However, it is apparent in thin section that this is merely a variant of mesh-textured serpentine (Figs. 3A–3C). The anastomosing foliation is locally oblique and/or perpendicular to the elongation directions of the porphyroclasts (e.g., 20° in Sample 153-920D-4R-2, Piece 14; 90° in Sample 3R-1, Piece 12). Serpentine pseudofibers in the serpentine bands of the anastomosing foliation are commonly perpendicular to the walls of the veinlets (Fig. 3D), suggesting that this pervasive structure is mainly a dilational fabric and not associated with non-coaxial deformation.

Development of mesh-textured serpentine is associated with the whole-rock serpentinization in the peridotites. It is a pseudomorphic texture after olivine and is generally composed of lizardite ± chrysotile, with accessory magnetite and/or brucite. Compositions of mesh rim and mesh center serpentine, hourglass mesh center serpentine, and a bastite rim around orthopyroxene are given in Table 2. These analyses show that pseudomorphic serpentines after olivine have compositions close to $Mg_3Si_2O_5(OH)_4$ with little substitution by Al or Fe, except in the bastite, which contains slightly more Al and Fe (Table 2; analysis 9). The majority of the rocks examined in this study are completely serpentinized, and mesh centers are composed of fine-grained lizardite + brucite (e.g., Fig. 3A). The presence of brucite in mesh-textured serpentinites is indicated by low silica contents in analyses of reddish brown mesh centers (Table 2; analysis 7). Backscattered electron imaging at high magnification was not able to resolve the individual phases in the mesh centers, suggesting that serpentine and brucite are extremely finely intergrown. Hourglass-textured lizardite within mesh centers is variably developed. True hourglass texture, where mesh rims are completely absent, was not found. Wicks and Whittaker (1977) suggested that hourglass mesh centers might develop at higher temperatures than isotropic mesh centers, as the latter are generally poorly crystalline. According to Wicks and Whittaker (1977), hourglass texture is mainly associated with recrystallization of serpentine within the chrysotile stability field. In samples from Hole 920B and 920D, the hourglass texture is limited to mesh centers, suggesting that whole-rock recrystallization after initial hydration was limited. Where serpentinization is incomplete, mesh centers are composed of olivine.

Very fine-grained acicular opaque minerals are closely associated with the development of mesh-textured serpentine. They occur in mesh centers, as shown in Figure 3B. Electron microprobe analysis of the acicular opaque minerals revealed iron, nickel, and sulfur peaks. As a quantitative analysis was not performed, the acicular crystals cannot be formally identified, although they may be pentlandite ($[Fe, Ni]_7S_8$). Analysis of several spots within the coarser-grained opaque minerals along partings between mesh textural units

Table 1. Stages of hydrothermal alteration and veining in the peridotites at Site 920.

Alteration event	Mineralogy	Width (mm)	Orientation/form	Remarks
Pervasive bulk-rock serpentinization	lizrdt + magnt ± bastite			Veinlets forming mesh texture and anastomosing foliation as part of the mesoscopic porphyroclastic fabric; wrapping porphyroclasts.
V1	serp + act ± chl ± talc	1–10	Discordant to parallel to the mantle fabric.	Postdates foliation; alteration halos (chl + serp); locally contain oblique serp or act fibers; may offset bastite grains.
V2	chrst + magnt	<1	Overprints mantle fabric and/or is locally orthogonal to it; discontinuous.	Network of thin, anastomosing veins in en echelon arrays; intensity dependent on porphyroclast abundance; contain wall-orthogonal chrysotile fibers.
V3	serp + magnt ±	>5	Randomly oriented, branching.	Contain crack-seal bands parallel to vein walls; wall-orthogonal chrysotile fibers showing antitaxial growth; include amorphous, submicroscopic serp + clay minerals.
V4	carb ± pyrite ± clay minerals	<1–3	Randomly oriented, branching, irregular.	Locally reactivated V3 veins; pyrite veins may locally contain hematite.

Notes: lizrdt = lizardite, magnt = magnetite, serp = serpentine, act = actinolite, chl = chlorite, chrst = chrysotile, and carb = carbonate.

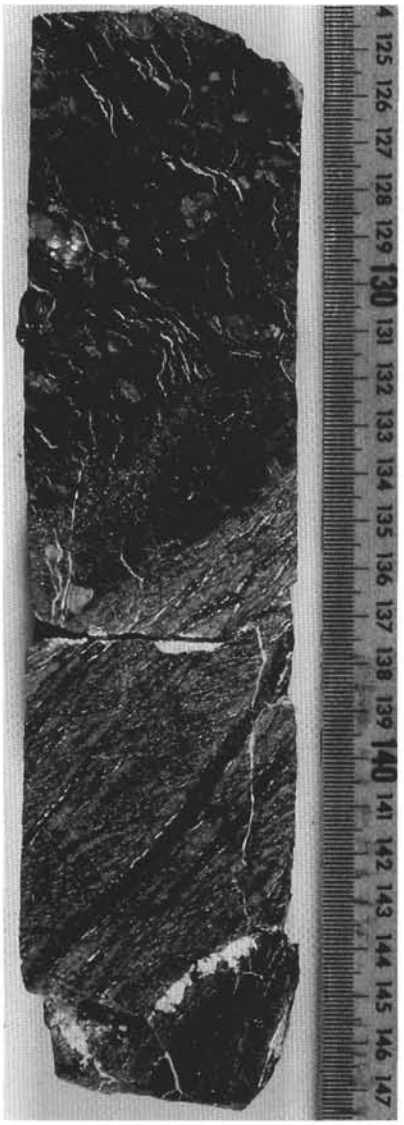

Figure 2. Serpentinized harzburgite with a pyroxene-depleted (dunitic) interval in the lower half of Sample 153-920B-12R-2, 124–148 cm. The harzburgitic upper part of the sample has a weak elongated porphyroclastic texture with a weak to moderately intense anastomosing foliation overprinted by thin, discontinuous, white, serpentine veins of the V2 generation. The anastomosing foliation dips to the right at 50°. A shear zone, starting at 134 cm and dipping to the left at 40°, separates the harzburgitic rock above from the dunitic interval below. The anastomosing foliation within the dunitic interval is characterized by a subparallel network of submillimetric serpentine + magnetite veinlets, producing a banded fabric in the rock. This banded fabric and the anastomosing foliation in the dunitic interval make a 75° angle with the V2 veins in the overlying harzburgite.

revealed no sulfur peak. This suggests that the opaque minerals in the mesh rim are likely to be composed of iron oxides only. In Sample 153-920D-19R-02, 108–114 cm, where an interlocking serpentine texture resulting from recrystallization occurs adjacent to a mesh texture, the acicular opaque minerals occur only within the mesh texture.

Hydrothermal Veins

Composite hydrothermal veins are widespread throughout the serpentinized peridotites and are typically dominated by serpentine minerals. These hydrothermal veins postdate the gabbroic and pyroxenitic magmatic veins, which are commonly discordant to the early, high-temperature, crystal-plastic fabric. Nearly consistent crosscutting relationships among different vein types, which display characteristic mineral assemblages and internal textures as observed in the core and in thin sections, suggest that there are mainly four discrete generations of hydrothermal veins that are associated with specific veining events. Mineralogy of the different vein generations was determined through hand-sample and thin-section studies, as well as X-ray diffraction and electron microprobe analyses of representative samples.

First-Generation Veins (V1)

The earliest hydrothermal veins (V1) are relatively rare in the core, and are composed of fibrous or very fine-grained chlorite and dark green serpentine with minor amounts of actinolite and talc (Shipboard Scientific Party, 1995). These veins are generally 1 to 3 mm in width, and are commonly highly discordant to the anastomosing foliation. Narrow (submillimetric) alteration halos consisting of chlorite ± serpentine ± amphibole form a diffuse zone in the bounding wallrock along these veins. Limited recrystallization has taken place in these diffuse zones; talc also occurs along some vein margins. Some of the V1 veins contain γ-serpentine fibers oblique to the vein walls, forming slip-fiber veins (Fig. 4A). They are commonly 1 to 3 mm in width and may crosscut bastite grains displaying shearing within and across them (Fig. 4B). They represent the only examples of slip-fiber veins found in this study; all other hydrothermal veins are pure extension veins. Compared with later veins and to the early pseudomorphic serpentine, the serpentine forming the slip fiber veins is relatively iron rich. FeO content ranges from 4.55 to 5.76 wt%.

Three analyses of the first-generation (V1) veins are included in Table 3 (analyses 9, 10, and 11); the Al content suggests that they are a low Fe chlorite, probably clinochlore. Thin-section studies have also revealed a single occurrence of prismatic apatite (0.1–0.25 mm long) and broken zircon crystals within one of the V1-generation veins. The existence of apatite and zircon was confirmed by electron-microprobe analysis (Sample 920B-5R-01, 58–62 cm; Fig. 5). The origin of the apatite and zircon is unclear. However, the chlorite vein in which they occur lies adjacent to a rodingitized gabbro vein, and the apatite and zircon are likely to be associated with late-stage gabbro crystallization. Apatite and zircon have previously been identified in gabbros from ODP Hole 735B (Stakes et al., 1991; Vanko and Stakes, 1991) and in gabbroic veins and dikelets in serpentinized peridotites dredged in the Mid-Atlantic Ridge axial valley at 15°37′N and 16°52′N (Cannat et al., 1992), and are found as accessory phases in the gabbroic veins in Site 920 peridotites (Shipboard Scientific Party, 1995). It is difficult to make any conclusions based on a single vein; however, as the apatite occurs within the earliest (V1) veins, the gabbro with which they are probably associated was intruded before the earliest stages of serpentine veining.

Recrystallization Zones

Recrystallization of serpentine locally occurs along the margins of V1 veins (Fig. 6), and produces a fine-grained interlocking texture along submillimeter planar zones or fan-shaped bundles of bladed serpentine crystals. The latter texture is shown in Figure 6A, where serpentine blades have grown along the boundary of an earlier chlorite + serpentine vein. Recrystallization only occurs within completely serpentinized sections of the peridotite and is relatively common, although extremely limited in extent. As recrystallization has also affected several of the slip-fiber veins, it is constrained to postdate V1 veining. Interlocking textures in serpentinites are generally indicative of prograde metamorphism (O'Hanley, 1991). The bladed habit and sweeping extinction parallel to the length of the blade are characteristic of antigorite (Fig. 6B), but the presence of antigorite could not be confirmed by X-ray diffraction because of the limited extent of recrystallization. The analyses of serpentine with interlocking textures given in Table 3 show that FeO content ranges from 4.0 to 6.22 wt%, which is generally higher than the FeO content of the pseudomorphic serpentinites.

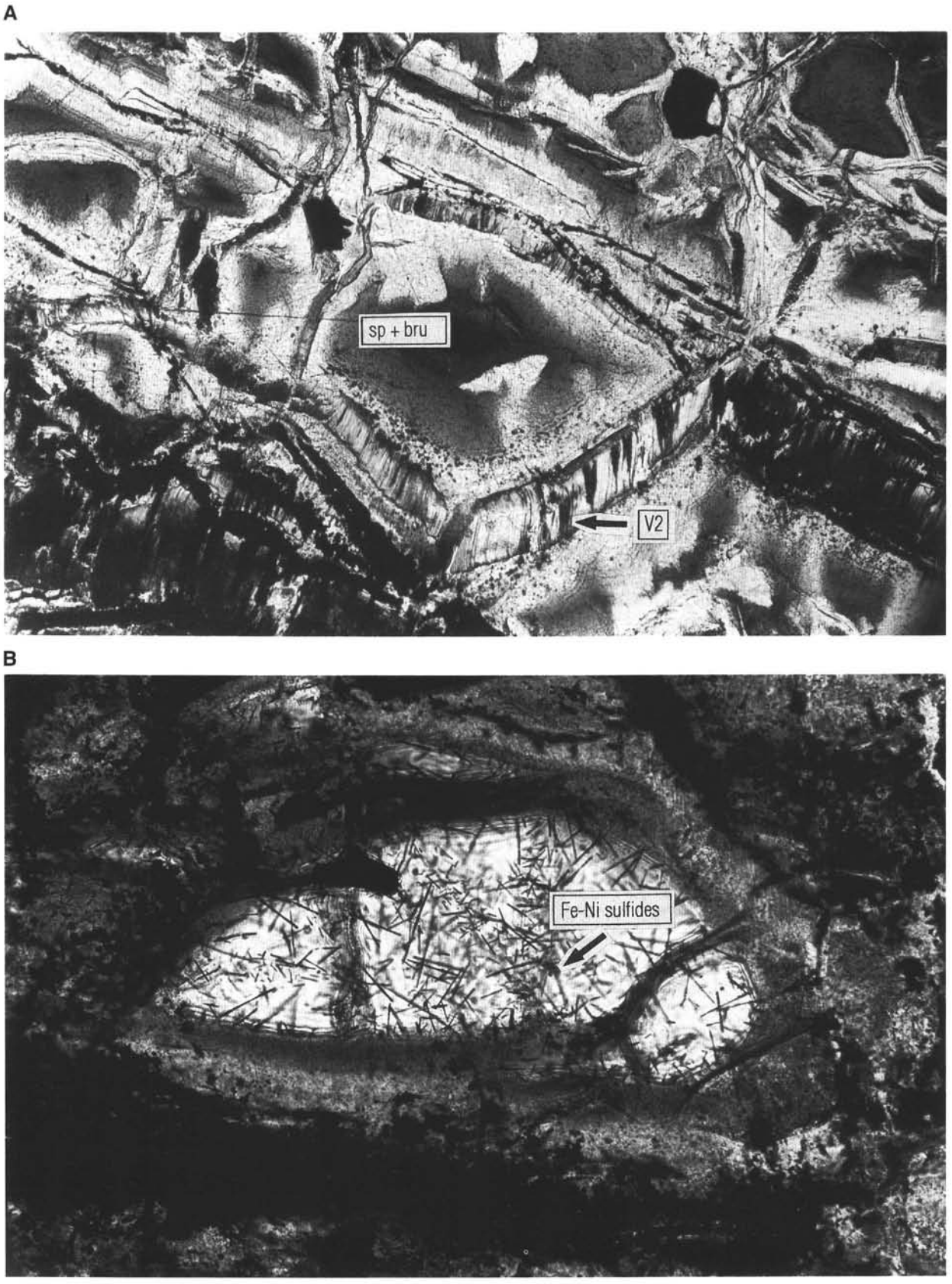

Figure 3. Photomicrographs of serpentinization textures in the peridotites from Holes 920B and 920D. **A.** Mesh texture serpentine + brucite. Mesh rim is composed of lizardite (colorless), whereas mesh center (dark) is composed of finely intergrown serpentine + brucite. Fibrous chrysotile extension vein follows the margins of mesh cell. Sp + bru = mesh textured serpentine + brucite. Plane-polarized light. Field of view is 2 mm long. Sample 153-920B-12R-2, 143–147 cm. **B.** Acicular Fe-Ni sulfides within mesh texture. Sulfides occur within mesh center serpentine. Plane-polarized light. Field of view is 1 mm long. Sample 153-920B-1W-1, 91–98 cm.

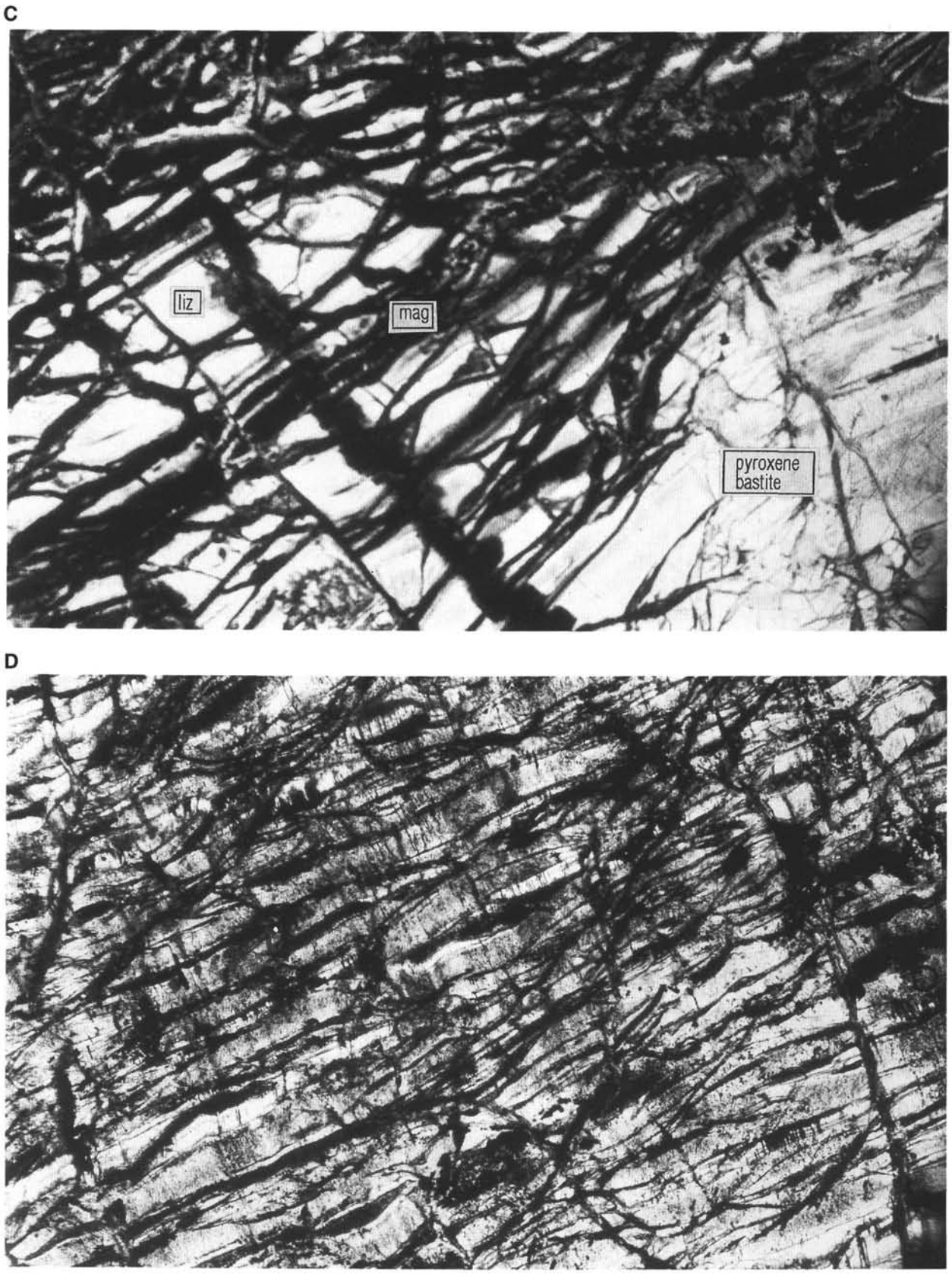

Figure 3 (continued). **C.** Elongate mesh texture developed adjacent to pyroxene bastite (lower right corner). Subparallel stringers of magnetite are developed along partings between elongate mesh cells, giving the rock a banded appearance; liz = lizardite, mag = magnetite. Plane-polarized light. Field of view is 3 mm long. Sample 153-920D-22R-5, 65–69 cm. **D.** Elongate mesh texture with mesh rim structure preferentially developed in one orientation. Mesh centers are almost absent. Plane-polarized light. Field of view is 3 mm long. Sample 153-920D-22R-5, 65–69 cm.

Table 2. Serpentine compositions from pseudomorphic serpentine textures in the peridotites from Hole 920B.

Analysis:	1	2	3	4	5	6	7	8	9
Texture:	Mesh center	Mesh center	Mesh rim	Hourglass mesh center	Mesh rim	Mesh center	Mesh center	Mesh rim	Bastite
SiO_2	41.286	42.506	41.089	41.562	41.498	42.894	24.057	40.407	39.134
TiO_2	0	0	0	0	0	0	0	0	0
Al_2O_3	0.452	0.882	0.502	1.582	0.361	0.323	0.348	0.325	3.642
FeO	2.053	2.234	3.840	4.643	1.963	1.735	4.229	1.822	4.744
MnO	0.039	0.045	0.024	0.109	0.043	0.04	0.258	0.063	0.137
MgO	40.216	40.345	39.87	37.99	40.399	40.198	55.968	40.233	36.003
CaO	0.011	0	0	0	0	0	0	0	0
Na_2O	0.011	0.015	0	0.061	0.016	0.023	0	0.001	0
K_2O	0.022	0	0	0	0	0.01	0	0	0
Total	84.09	86.03	85.33	85.95	84.28	85.22	84.86	82.85	83.66
Si	3.983	4.004	3.947	3.970	3.992	4.063	2.521	3.958	3.846
Ti	0	0	0	0	0	0	0	0	0
Al	0.051	0.098	0.057	0.178	0.041	0.036	0.042	0.038	0.422
Fe	0.166	0.176	0.309	0.371	0.158	0.138	0.364	0.149	0.390
Mn	0.003	0.004	0.002	0.009	0.004	0.003	0.023	0.005	0.012
Mg	5.784	5.665	5.710	5.408	5.792	5.676	8.510	5.874	5.274
Ca	0.001	0	0	0	0	0	0	0	0
Na	0.002	0.002	0	0.012	0.003	0.004	0	0	0
K	0.002	0	0	0	0	0.001	0	0	0

Notes: All formulas calculated on the basis of 14 oxygens. Analyses 1–3 are from Sample 153-920B-1W-1, 48–52 cm. Analyses 4 and 5 are from Sample 153-920B-5R-2, 67–71 cm. Analyses 6–8 are from Sample 153-920B-12R-2, 143–147 cm. The low silica content in analysis 7 is probably caused by abundant brucite in this sample. Analysis 9 is a bastite rim around orthopyroxene from Sample 153-920B-5R-1, 58–62 cm.

Second-Generation Veins (V2)

The second-generation veins (V2) are the most common throughout the peridotites, and contain very thin serpentine fibers that display a relatively high birefringence and undulose extinction. Fine-grained iron oxide minerals (magnetite) are intergrown between the serpentine fibers. V2 veins occur as a network of thin (up to 3 mm) veins, and are commonly parallel to the anastomosing foliation; they locally form narrow (~5 cm), en echelon arrays subparallel to the trace of the foliation. They may locally occur along the trace of the preexisting V1 veins (e.g., Sample 153-920B-1W-1, 48–60 cm). The occurrence of these veins is heterogeneous down the core, with the highest abundances corresponding to the areas of relatively high orthopyroxene porphyroclast content. They form isolated and discontinuous rings around the porphyroclasts (Fig. 7), and also occur as semicontinuous en echelon swarms containing alternating bands of black magnetite-rich and white serpentine-rich veins. The white serpentine veins are thickest at the widest point of the porphyroclasts that deflect the vein traces (Fig. 8). Orientations of the V2 veins vary considerably in the core. In some places they form subhorizontal (with respect to the vertical core axis) planar features (e.g., Sample 153-920D-12R-1, 1–13 cm; Fig. 9A), whereas in other places they are nearly subvertical (e.g., Sample 153-920D-14R-5, 105–112 cm; Fig. 9B). In some pieces, they also form two subperpendicular arrays (e.g., Sample 153-920D-4R-3, Piece 5).

Serpentine fibers in the V2 veins are generally perpendicular to the vein walls, suggesting a pure extension origin of these veins. X-ray diffraction analyses suggest that the fibers are made of chrysotile (i.e., Samples 153-920B-9R-2, 111–115 cm; 153-920D-22R-5, 65–69 cm; Figs. 10A, 11A), which has low Al and Fe contents (Table 4; analyses 4–6). In many thin sections, multiple and subparallel chrysotile veins are formed by exploiting preexisting planes of weakness within the serpentinite, such as mesh rims (Fig. 3A). Multiple subparallel extensional veins suggest that this stage of the serpentinization was associated with a volume increase. A transition from slip-fiber (V1) to cross-fiber extension veins (V2) also indicates higher pore fluid pressures and expansion.

Third-Generation Veins (V3)

Third-generation veins (V3) are characterized by more discrete, commonly branching, planar veins that are composed of pale green-white serpentine with lesser amounts of aragonite, pyrite, magnetite, and clay minerals. V3 veins generally crosscut the fibrous V2 veins (Fig. 12). They are typically wider than 5 mm, and are locally crosscut and displaced by sigmoidal arrays of up to 4 mm-wide, aqua green to light blue (in hand-sample) serpentine veins (Fig. 13). These aqua veins contain amorphous, submicroscopic serpentine ± clay minerals. Rare mutual crosscutting relations between the discrete V3 veins and the sigmoidal, aqua veins suggest that either these two vein types are temporally associated or there is more than one generation of V3 veins. The discrete V3 veins generally have up to several millimeter-wide, dark gray-blue alteration halos (Fig. 13).

Although the V3 veins are massive in hand specimen, in thin section, particularly under crossed polars, they display a banded internal texture with bands parallel to the vein margins. In plane-polarized light, V3 veins are generally reddish brown; the bands show an alternation of light and dark colors and are crenulated along their traces (Fig. 14A). Individual bands have a pseudofibrous internal fabric (Fig. 14B) characteristic of antitaxial growth of vein-filling serpentine minerals (Ramsay and Huber, 1983). Some veins contain small inclusions and fragments of wall-derived material within and along the bands (Fig. 14A), indicating the incorporation of the host rock into the veins during their successive openings along the vein-wall contact. This inferred periodic opening and crack filling of the V3-generation veins suggest a crack-seal mechanism of formation (Ramsay, 1980; Ramsay and Huber, 1983).

X-ray diffraction data indicate that the main serpentine mineral in the V3 veins is lizardite (i.e., Samples 153-920D-16R-6, 59–64 cm; 22R-5, 65–69 cm; 920B-1W-1, 48–52 cm; Figs. 10B, 11B). Electron microprobe analyses of selected veins are given in Table 4. Generally, the composition of the V3 veins is similar to that of the fibrous chrysotile V2 veins. Both V2 and V3 veins have chemical compositions close to the composition of the early pseudomorphic serpentine textures with low FeO and Al_2O_3 contents. FeO content ranges from 2.1 to 26 wt% and Al_2O_3 content ranging from 0.8 to 2.55 wt%.

Fourth-Generation Veins (V4)

Fourth-generation (V4) veins form the latest generation of veining in the serpentinized peridotites and contain infilling of carbonate minerals + clay minerals, carbonate minerals + pyrite, and/or pyrite (Fig. 15). V4 veins commonly occur as isolated, individual veins and are thin (<1 mm to 1 mm) and irregular in geometry with random orientation. Pyrite-rich veinlets occur as very thin, discontinuous stringers. The V4 veins crosscut the V2 and V3 veins (Fig. 12) and reacti-

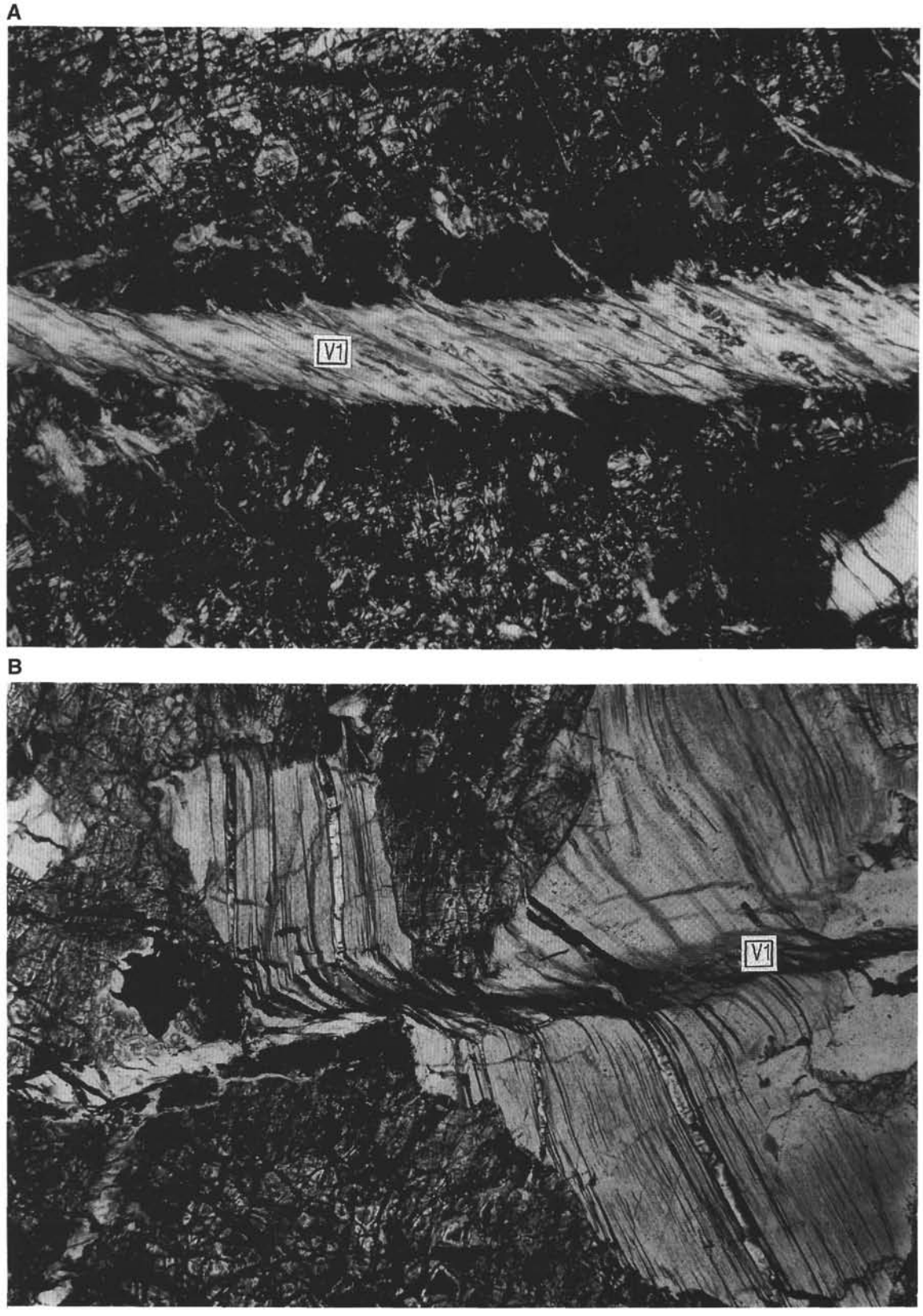

Figure 4. **A.** Slip-fiber vein (V1) composed of chlorite + serpentine + actinolite ± talc in Sample 153-920B-9R-2, 111–115 cm. The orientation of vein-filling fibers oblique to the walls suggests left-lateral shear during vein development. Crossed polars. Field of view is 3 mm long. **B.** Left-lateral shearing along a chlorite + serpentine V1 vein across a bastite grain in the same sample as above. Plane-polarized light. Field of view is 3 mm long.

Table 3. Composition of representative V1 (chl + srp ± act ± talc) veins and recrystallized serpentine zones in Hole 920B.

Analysis:	1	2	3	4	5	6	7	8	9	10	11
Texture:	Recrystallized serpentine	Recrystallized serpentine	Recrystallized serpentine	Recrystallized serpentine	Recrystallized serpentine	Recrystallized serpentine	Recrystallized serpentine	Recrystallized serpentine	Chlorite	Chlorite	Chlorite
SiO_2	41.08	40.698	41.781	41.888	41.252	41.516	42.33	41.958	28.869	30.679	33.038
TiO_2	0	0	0	0	0	0	0	0	0	0	0
Al_2O_3	0.322	0.252	0.114	0.28	0.987	0.821	0.284	0.426	18.859	16.889	12.32
FeO	6.222	6.219	4.352	4.041	5.494	5.933	5.812	3.721	13.532	10.363	6.48
MnO	0.055	0.069	0.013	0.032	0.221	0.202	0.198	0.08	0.409	0.338	0.03
MgO	37.172	37.284	39.253	38.929	36.437	36.467	36.589	39.1660	24.516	28.059	32.742
CaO	0	0	0	0	0	0	0	0	0	0	0
Na_2O	0.034	0.03	0	0	0	0	0	0.043	0	0.03	0
K_2O	0	0	0	0	0.005	0	0.003	0	0	0.003	0
Total	84.88	85.09	85.51	85.17	84.4	84.94	85.22	85.39	86.18	86.36	84.61
Si	4.01	3.971	4.008	4.025	4.029	4.037	4.095	4.016	5.803	6.048	6.509
Ti	0	0	0	0	0	0	0	0	0	0	0
Al	0.037	0.029	0.013	0.032	0.114	0.094	0.032	0.048	4.468	3.925	2.861
Fe	0.508	0.507	0.349	0.324	0.449	0.483	0.470	0.298	2.275	1.708	1.068
Mn	0.004	0.005	0.001	0.002	0.018	0.016	0.016	0.007	0.069	0.056	0.005
Mg	5.408	5.500	5.613	5.576	5.304	5.285	5.276	5.588	7.346	8.245	9.616
Ca	0	0	0	0	0	0	0	0	0	0	0
Na	0.006	0.005	0	0	0	0	0	0.008	0	0.012	0
K	0	0	0	0	0.001	0	0.001	0	0	0.001	0

Notes: Serpentine and chlorite formulas calculated on the basis of 14 and 28 oxygens, respectively. Analyses 1–6, 9, and 10 are from Sample 153-920B-5R-1, 58–62 cm. Analyses 7, 8, and 11 are from Sample 153-920B-5R-2, 67–71 cm; chl = chlorite, srp = serpentine, act = actinolite.

vate some of the early serpentine + chlorite ± actinolite ± talc (V1) veins.

Electron microprobe analysis of the V4 veins indicate that the vein sulfides contain iron; no nickel was detected. Therefore, the late-stage vein sulfides are geochemically distinct from those associated with the mesh-textured serpentinite. The margins of pyrite-bearing veins are commonly stained red, indicating some oxidation of the sulfides to hematite. The composition of the clay mineral associated with the pyrite is given in Table 4 (analysis 10).

DISTRIBUTION AND ORIENTATION OF HYDROTHERMAL VEINS IN HOLES 920B AND 920D

The occurrence of hydrothermal veins and alteration minerals and the documented crosscutting relations of different vein generations are the same in Holes 920B and 920D. There is a strong correspondence between the distribution and orientation of the crystal-plastic deformation fabric and extensional fibrous chrysotile veins (V2) in the core from both holes. The anastomosing foliation overprints the high-temperature mantle fabric, and is in turn accentuated by the extensional V2 veins. Consequently, all three fabric elements commonly display similar orientations in the core.

Different fabric elements (i.e., mesoscopic porphyroclastic fabric, anastomosing serpentine foliation) and vein generations were measured in the core using the method described in Shipboard Scientific Party (1995). A total of 344 structural observations and measurements from individual pieces of core that had been sampled for paleomagnetism were reoriented using the declination of the stable remanence (see Hurst et al., this volume). The mesoscopic porphyroclastic foliation displays a mean attitude of 325°/29° NE in Holes 920B and 920D, whereas the anastomosing foliation slightly changes from a mean attitude of 338°/37° NE in Hole 920B to 345°/45° NE in Hole 920D (Hurst et al., this volume). The extensional fibrous chrysotile (V2) veins cluster around a mean attitude of 336°/29° NE for both holes. This orientation overlaps the corrected strike and dip measurements of the anastomosing foliation and the mesoscopic porphyroclastic fabric. The early V1 veins (chlorite + serpentine ± actinolite ± talc) display a wide range of dips in both holes, but the majority of them have northwest strikes. The crack-seal serpentine veins (V3) have a wide scatter of azimuths, but in general show steep to moderate dips to the east. The dip angles of V3 veins are consistently steeper than those of the V1 and V2 vein generations in Hole 920B.

Downhole variations in the intensity and orientation of the fabric elements and vein generations show no significant trends in Holes 920B and 920D. The anastomosing foliation is more pronounced in a number of intervals in Samples 153-920B-3R-1 (Piece 1), 4R-1 (Piece 4), 5R-3 (Piece 1), 12R-1 (at the base), and 12R-2 (at the base)(Shipboard Scientific Party, 1995). These intervals either correspond to boundaries between different lithological units or to an increase in the porphyroclast content in the serpentinized peridotite. In Hole 920D the anastomosing foliation is less intense than in Hole 920B, and is strongest in the upper half of the core, although absent in several intervals below 120 mbsf (Shipboard Scientific Party, 1995). Mimicking the mesoscopic porphyroclastic fabric, the dip angles of the anastomosing foliation decrease towards the bottom of Hole 920D.

Figures 16 and 17 show downhole variations in dip and strike angles for different vein generations and the mesoscopic porphyroclastic fabric in Holes 920B and 920D. Both V2 and V3 veins display moderate to steep dip angles at 62 and 94 mbsf in Hole 920B. Figure 17 shows that the attitudes of mesoscopic porphyroclastic fabric (Pf) and extensional fibrous veins (V2) correspond better at depths down to 100 mbsf, below which this correspondence dissipates as a result of the scatter in V2 vein orientation. Both V1 and V3 veins display more scattered strike and dip angles towards the bottom of Hole 920D. In general, all structural elements (foliations and different vein generations) are shallower in Hole 920D than their counterparts in Hole 920B.

TECTONIC IMPLICATIONS FOR HYDROTHERMAL ALTERATION AND ASSOCIATED BRITTLE DEFORMATION: DISCUSSION AND CONCLUSIONS

Mode of Alteration

The medium- to coarse-grained porphyroclastic texture in the serpentinized harzburgites at Site 920 represents a mantle fabric that formed during recrystallization and deformation at minimum temperatures of 800° –1000°C (Kirby, 1983; Cannat et al., 1992). Mineralogical evidence for high-temperature (>500°C) interaction with hydrothermal fluids is generally minor or absent in the peridotites, except in localized mylonite zones (Shipboard Scientific Party, 1995). Ribbons of metagabbroic and metapyroxenitic material in these mylonitic zones contain fine-grained hornblende and are interfingered between the recrystallized ultramafic assemblages. These mineralogical and textural relations suggest that shearing and limited hydration occurred at minimum temperatures of 700°–900°C in the upper man-

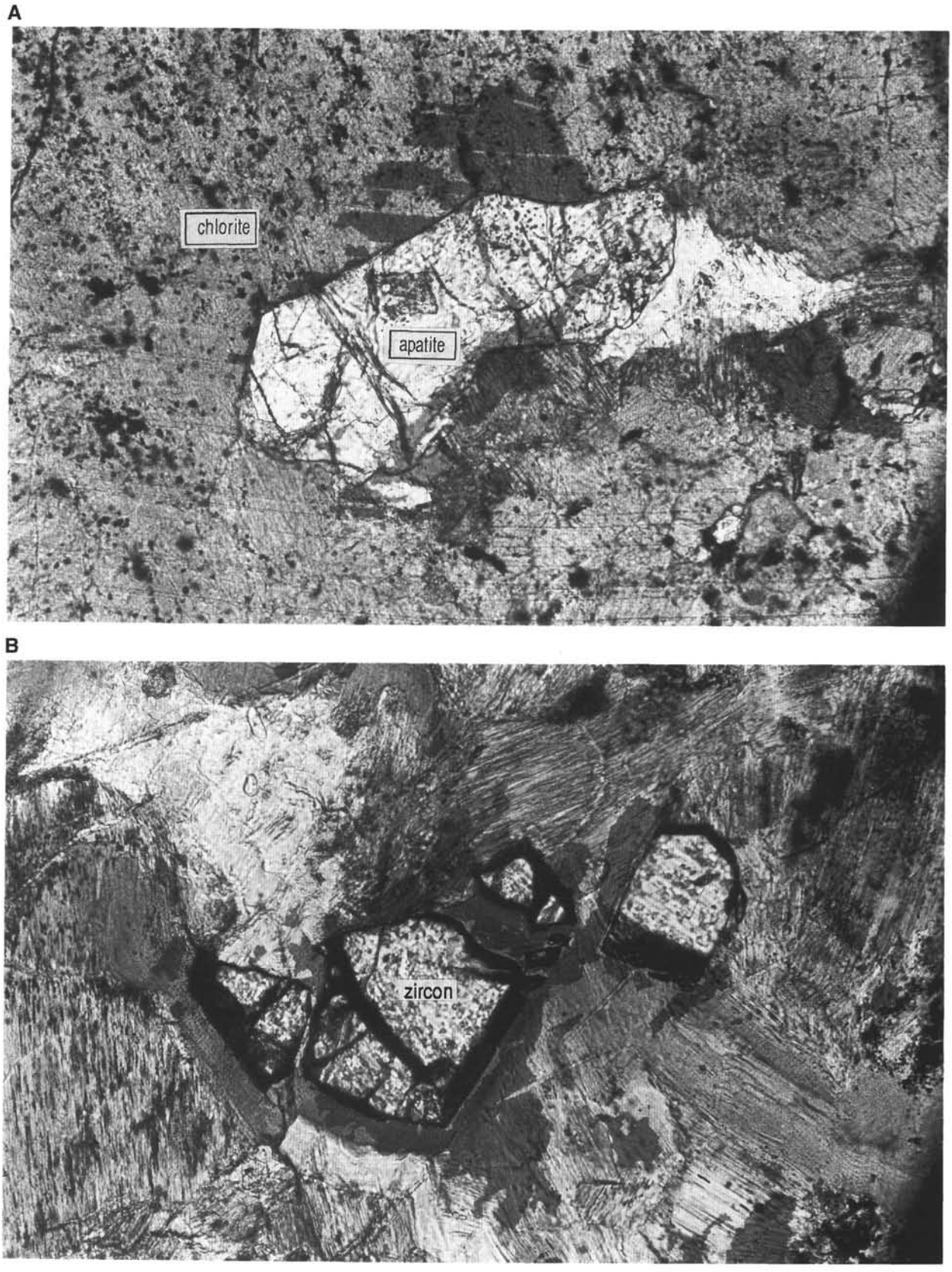

Figure 5. Photomicrographs of accessory minerals and textures within serpentine veins in Hole 920B. **A.** Apatite crystal within a chlorite + serpentine vein (V1). Apatite crystal is 0.75 mm in length. Plane-polarized light. Sample 153-920B-5R-1, 58–62 cm. **B.** Broken zircon crystal within chlorite in the same V1 vein as in A. Area of photograph is adjacent to the apatite crystal in B. Zircon crystal is crosscut by massive serpentine vein of V3 generation. Plane-polarized light. Field of view is 1 mm long.

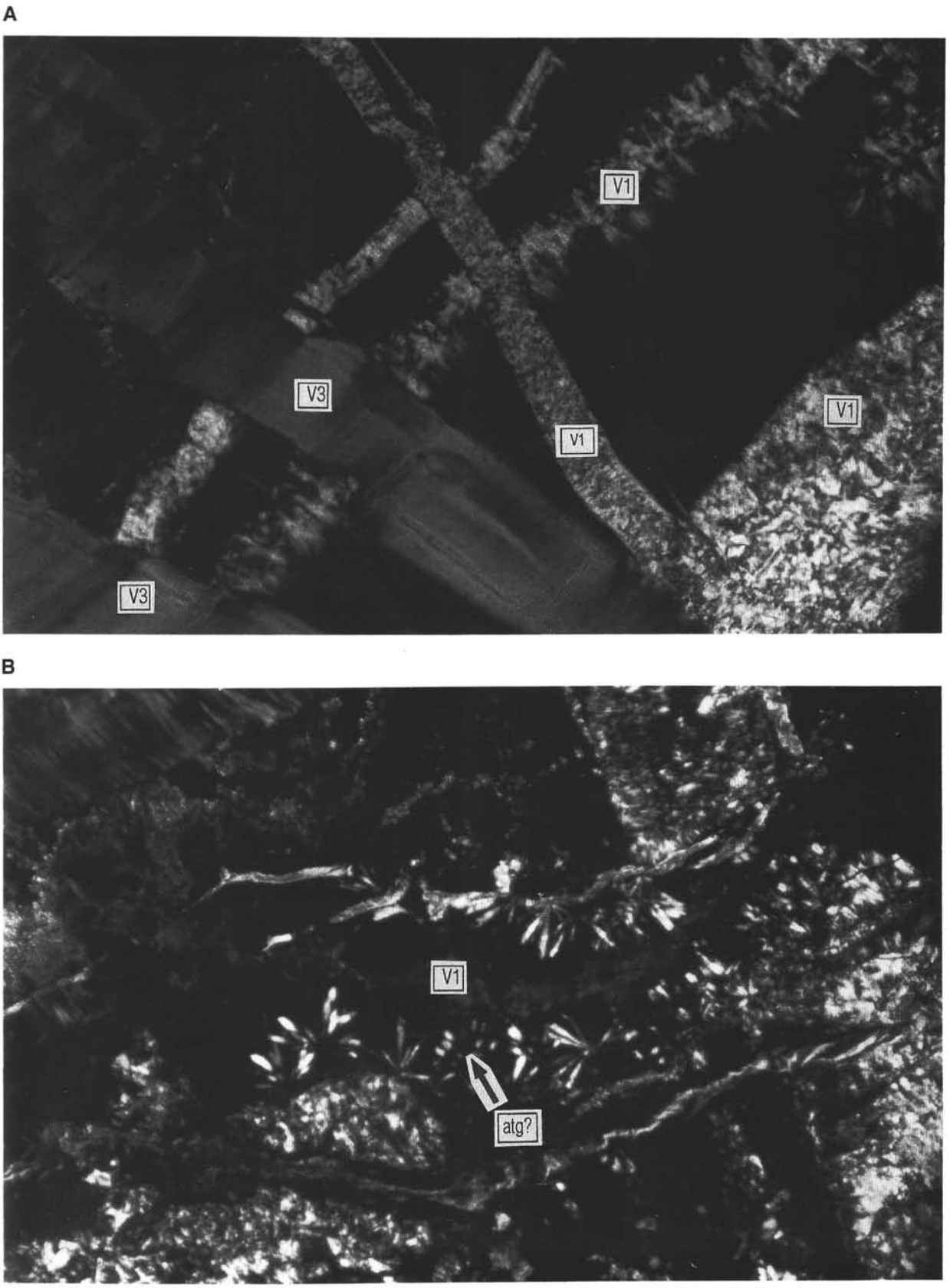

Figure 6. **A.** Recrystallized zones of serpentine within and along the early V1 veins show interlocking and bladed textures. They are crosscut by two banded serpentine veins of V3 generation. Crossed polars. Field of view is 1 mm long. Sample 153-920B-5R-2, 67–71 cm. **B.** Fan-shaped bundles of bladed serpentine (antigorite? = atg?) along boundary of earlier formed chlorite + serpentine vein (V1). Plane-polarized light. Field of view is 1 mm long. Sample 153-920B-5R-1, 58–62 cm.

Figure 7. Discontinuous rings of fibrous chrysotile veins (V2) wrapping around the porphyroclasts in serpentinized harzburgite. Some of these V2 veins are reactivated by massive wispy serpentine veins of the V3 generation that also crosscut at high angles a branching, aqua blue massive serpentine (V3) vein between 39 and 44 cm (Sample 153-920B-8R-3, 31–48 cm).

tle (Spear, 1981). The existence of pale green amphibole, chlorite, and chrysotile + lizardite as retrograde mineral assemblages in these shear zones indicates that interaction with hydrothermal fluids continued down to at least greenschist facies conditions (Shipboard Scientific Party, 1995). Alteration of orthopyroxene to talc and cummingtonite in polymineralic lenses and adjacent to magmatic veins suggests that hydrothermal fluids penetrated at least locally into the peridotites under amphibolite to greenschist facies conditions (Shipboard Scientific Party, 1995). The relative absence of high-temperature secondary phases may be a result of either nonpervasive, high-temperature fluid circulation in the harzburgites, or the widespread overprinting of high-temperature phases by the whole-rock serpentinization associated with circulation of lower temperature fluids.

The pervasive background alteration and whole-rock serpentinization in the ultramafic rocks at Site 920 are associated with the formation of the anastomosing foliation and polymineralic veins. Closely spaced, parallel, serpentine bands and veinlets of the anastomosing foliation has resulted in intense static serpentinization of the peridotites. The occurrence of wall-perpendicular serpentine fibers in bands and veinlets of the anastomosing foliation indicates that the large volume change associated with this background serpentinization was strongly anisotropic. Lithological variations in the peridotites seem to have affected the intensity of the foliation and related alteration.

Intrusion of gabbroic to pyroxenite veins and veinlets in the peridotites represents a phase of magmatic veining before the formation of hydrothermal veins (Shipboard Scientific Party, 1995). The magmatic veins are commonly intensely altered, and the primary mineralogy is partially to entirely replaced by a combination of brown amphibole, tremolite, and actinolite; prehnite, epidote, zoisite, chlorite, and hydrogrossular garnet constitute the most common secondary minerals in the gabbroic veins (Shipboard Scientific Party, 1995). This mineralogy is consistent with alteration associated with Ca-enriched fluids under greenschist facies conditions at temperatures of 300°–400°C.

Polymineralic hydrothermal veins in the peridotites represent successive episodes of fracturing and hydration associated with brittle deformation in decreasing temperatures. The early V1-generation veins containing chlorite + serpentine ± actinolite ± talc minerals and oblique slip-fibers indicate dilation and contemporaneous shearing associated with tension that enhanced fluid circulation into the peridotites under lower greenschist facies conditions. The occurrence of apatite and zircon in some of the V1 veins suggests that early fluids were enriched in extremely incompatible elements. The absence of a gabbro and/or gabbroic veins in proximity to these V1 veins suggests that apatite and zircon are likely to have a hydrothermal origin. However, the existence of these minerals in gabbroic veins and veinlets in the serpentinized peridotites also indicates their magmatic origin and derivation from fluids fractionated from melts of evolved compositions. Therefore, some early generation V1 veins may be spatially and temporally associated with pervasively altered magmatic veins and/or they may represent some pervasively altered magmatic veins. Cannat et al. (1992) described gabbroic dikelets and veins in serpentinized peridotites dredged in the Mid-Atlantic Ridge axial valley at 15°37′N and 16°52′N that contain a zircon- and oxide-bearing assemblage of clinopyroxene and plagioclase. The primary phases in these magmatic intrusions are extensively altered to chlorite, actinolite, tremolite, phlogopite, and talc. Cannat et al. (1992) suggested that the hydrothermal alteration of the gabbroic veins and dikelets had begun before and at higher temperatures than the pervasive hydration of their host peridotite. Recrystallization spatially associated with the early V1-generation veins was probably caused by reheating along permeable zones, such as newly developed cracks or the preexisting veins, by discharging hydrothermal fluids after retrograde serpentinization had taken place. In the model of serpentinization proposed by Sanford (1981), recrystallization of initially formed lizardite + chrysotile to antigorite could occur without an increase in temperature if lizardite + chrysotile formed metastably at temperatures of 200°–450°C. However, temperatures remained below 350°C because there is no evidence for recrystallization of olivine in the serpentinized peridotites examined in this study. The occurrence of chrysotile and lizardite in the V2 and V3 vein sets, respectively, indicates that much of the hydration in the ultramafic rocks took place at temperatures below 350°C (Fig. 18).

Temperatures of Serpentinization

Experimental, field, and petrographic studies have confirmed that the serpentine mineral antigorite has a distinct stability field, and that it is generally stable to higher temperatures than chrysotile and lizardite (see Evans et al., 1976; and Chernosky et al., 1988, for a review of experimental and field data). Although all the serpentine group minerals can be approximated by the formula $Mg_3Si_2O_5(OH)_4$, antigorite has a distinct, slightly different chemical composition, $Mg_{2.813}$, $Si_2O_5(OH)_{3.647}$ (Kunze, 1958), and cannot be considered a polymorph of lizardite or chrysotile. At low pressures the upper stability limit of antigorite is given by the reaction antigorite = forsterite + talc + water, which occurs at around 500°C for a pressure of 2 kbar (Fig. 18). Recent experimental work (Ulmer and Trommsdorff, 1995) has indicated that at very high pressures antigorite may be stable to higher temperatures (e.g., ~720°C at 2 GPa), and field studies have documented the occurrence of antigorite within eclogite facies assemblag-

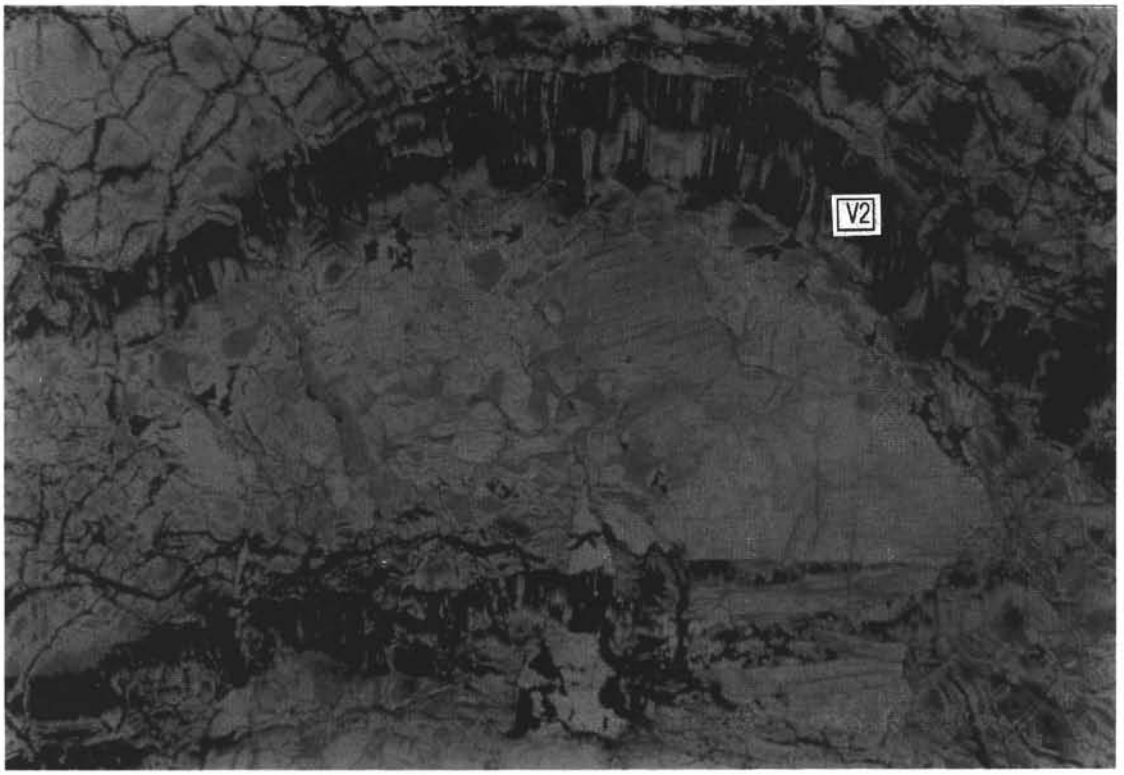

Figure 8. Fibrous chrysotile and magnetite veins (V2) deflecting around an orthopyroxene and olivine porphyroclast partially pseudomorphed by bastite and serpentine, respectively. Chrysotile fibers are perpendicular to the vein walls, suggesting dilation via pure extension (Sample 153-920B-3R-1, 108–115 cm). Plane-polarized light. Field of view is 6 mm long.

es (Scambelluri et al., 1995). However, such high-pressure conditions are more applicable to subduction zones than to mid-ocean ridge environments and, therefore, we prefer an upper temperature limit of around 500°C for antigorite for $P(H_2O)$ of 2 kbar. A lower limit for antigorite stability, in the absence of brucite, is defined by the reaction chrysotile = brucite + antigorite (Fig. 18).

Field and experimental data have confirmed the existence of a stability field for chrysotile at temperatures below about 200°C (Evans et al., 1976). The stability field for lizardite is less well defined. Given that lizardite and chrysotile occur commonly together in natural samples and that they have a similar chemical composition, they are generally considered to have similar pressure-temperature stabilities. It is known, however, from experimental studies that coupled substitution of Al for Mg and Si in the lizardite structure reduces the misfit between the octahedral and tetrahedral layers and substantially increases the stability of lizardite (Chernosky, 1973; Caruso and Chernosky, 1979). Experiments involving synthetic lizardite containing 3.7 wt% Al_2O_3 and 9.25 wt% Al_2O_3 resulted in upper stability limits for lizardite at temperatures of ~500° and 580°C, respectively, at 2 kbar $P(H_2O)$. However, the majority of naturally occurring lizardites have lower Al contents, and a stability field for Al-free lizardite has not been defined. Al-free lizardite probably only forms stably at very low temperatures (below 200°C).

Wicks and Whittaker (1977), in a comprehensive study of serpentine textures, noted that formation of antigorite directly from olivine was extremely rare, a clear example being found in only one sample out of over 1300 thin sections they studied. Observations of natural samples indicate that the most common retrograde serpentinization reaction produces lizardite from olivine. Experimental data of Moody (1976b) and Wegener and Ernst (1983) also indicate lizardite forming initially from olivine, with chrysotile only forming in experiments of longer duration, suggesting that the formation of lizardite is kinetically favored. The phase relationships in Figure 18 indicate that lizardite can only form metastably from olivine, except perhaps at very low $P(H_2O)$. However, it has been suggested (Sanford, 1981; O'Hanley et al., 1989) that as serpentinization is a water-consuming reaction, very low $P(H_2O)$ might be maintained at the reaction interface during initial serpentinization and that stable formation of lizardite might be possible. $P(H_2O)$ would only increase once serpentinization was complete. However, this hypothesis remains unconfirmed.

Oxygen-isotope geothermometry is in general agreement with the experimentally defined phase relationships. Wenner and Taylor (1971) reported temperatures of 85°–115°C for continental lizardite and chrysotile and temperatures of 130°C and 185°C for two oceanic lizardite and chrysotile samples. They also reported temperatures of 220°C to 460°C for continental antigorite and 235°C for a single oceanic antigorite. Although oxygen-isotope fractionation factors are not well defined for temperatures below 400°C, the temperatures derived by oxygen-isotope geothermometry by Wenner and Taylor (1971) indicate that lizardite and chrysotile form at lower temperatures than antigorite. However, the temperature at which lizardite may begin to form metastably from olivine can only be estimated. Figure 18 indicates that the lowest temperature at which forsterite may stably coexist with water, in the absence of talc, is approximately 400°C, defined by the reaction forsterite + water = antigorite + brucite (Evans et al., 1976). The metastable reaction forsterite + water = chrysotile + brucite (Johannes, 1968) occurs at a slightly lower temperature.

The initial formation of mesh texture serpentine in serpentinites in this study is estimated to have begun at temperatures around 350°–400°C, assuming metastable formation of a (low Al) mesh-textured lizardite + brucite. Brucite is found intimately intergrown with Al-poor serpentine in mesh centers (Fig. 3A), and is therefore assumed to be associated with the initial stages of serpentinization and formation of the mesh texture. Al-rich serpentine is found in orthopyroxene bastites (Table 2; analysis 9), and the Al_2O_3 content of 3.6 wt% suggests that it could have formed stably at temperatures close to 500°C. However, there is no clear evidence from petrographic observations that serpentinization of orthopyroxenes began before serpentiniza-

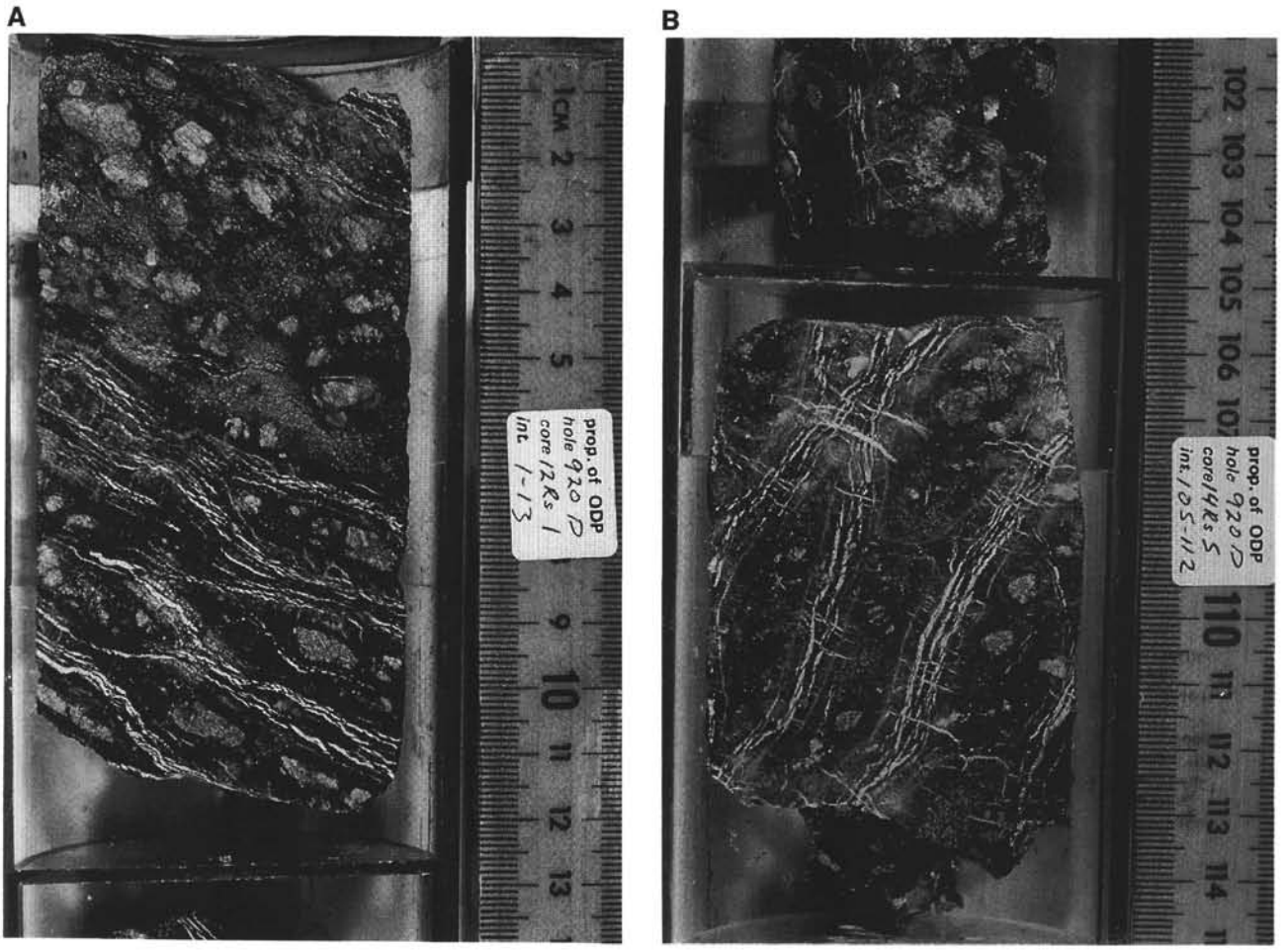

Figure 9. Downhole variations in the orientation of V2 (serpentine + magnetite) veins in the core. **A.** En echelon arrays of shallowly dipping (in the core reference frame), white, serpentine veins overprinting the anastomosing foliation that wraps around the elongated porphyroclasts. Sample 153-920D-12R-1, 1–13 cm. **B.** Continuous bands of white serpentine veins dipping at steep angles to the opposite direction of those in A. These V2 veins are cut by sigmoidal massive serpentine veins of the V3 generation (Sample 153-920D-14R-5, 105–112 cm).

tion of olivine. Minor recrystallization to an interlocking (antigorite?-bearing) texture occurs along vein boundaries (Fig. 6B). The recrystallization may be promoted by either an increase in temperature along the vein boundaries resulting from discharging hydrothermal fluids or the presence of a silica-bearing fluid, as a lowered Mg:Si ratio will favor the formation of antigorite, at temperatures within the stability field of antigorite (~200°–500°C).

Stable-isotope geothermometry on serpentine-magnetite mineral pairs from the early formed mesh texture and later chrysotile + magnetite extension veins (V2) might provide further information on temperatures of serpentinization. However, it should be noted that no temperatures above 200°C were reported for lizardite or chrysotile serpentinites in the stable-isotope study of Wenner and Taylor (1971). This is at odds with our estimation that serpentinization may have begun around 400°C. Further stable-isotope studies of detailed textural relationships within oceanic serpentinites would provide a larger data set with which to evaluate the temperature of initial serpentinization and later veining.

Spatial and Temporal Relations Between Hydrothermal Veining and Brittle Deformation

The pervasive low-temperature bulk-rock serpentinization and hydrothermal veining of Site 920 peridotites to form lizardite, chrysotile, and antigorite require infiltration of water into the rock to cause the hydration of the primary mineral phases. This suggests that the lower crust and the upper mantle in the MARK area had acquired high fracture permeability that resulted in downwelling of seawater to cause hydration and serpentinization. The high fracture permeability is interpreted to have been facilitated by lithospheric stretching and faulting under conditions of attenuated magmatism within the ridge axial region. Table 5 summarizes the inferred stages of brittle deformation and low-temperature hydrothermal alteration of the upper mantle during the tectonic evolution of the MARK area. Microstructural studies in dredged and drilled peridotites from the Mid-Atlantic Ridge axial valley (at 15°37′ N and 16°52′N) and the MARK area show that the low-stress, high-temperature asthenospheric deformation of the ultramafic rocks was followed by ductile flow under relatively high deviatoric stresses in lithospheric conditions (Cannat et al., 1992; Shipboard Scientific Party, 1995; Ceuleneer and Cannat, this volume). This ductile deformation predates the static serpentinization of the peridotites, and has been probably driven by stretching of the axial lithosphere along normal shear zones and faults, which in turn facilitated the tectonic uplift of the mantle-derived rocks (Cannat et al., 1992). Stretching and thinning of the axial lithosphere along normal faults resulting from tectonic extension in the absence of a magma chamber are likely to enhance brittle cracking down to the upper mantle and thus to facilitate the penetration of seawater along grain boundaries, causing extensive bulk-rock serpentinization and development of mesh texture, and subsequent veining.

Mesoscopic structural fabrics in the peridotite outcrops on the seafloor in the MARK area (on the western wall of the axial valley)

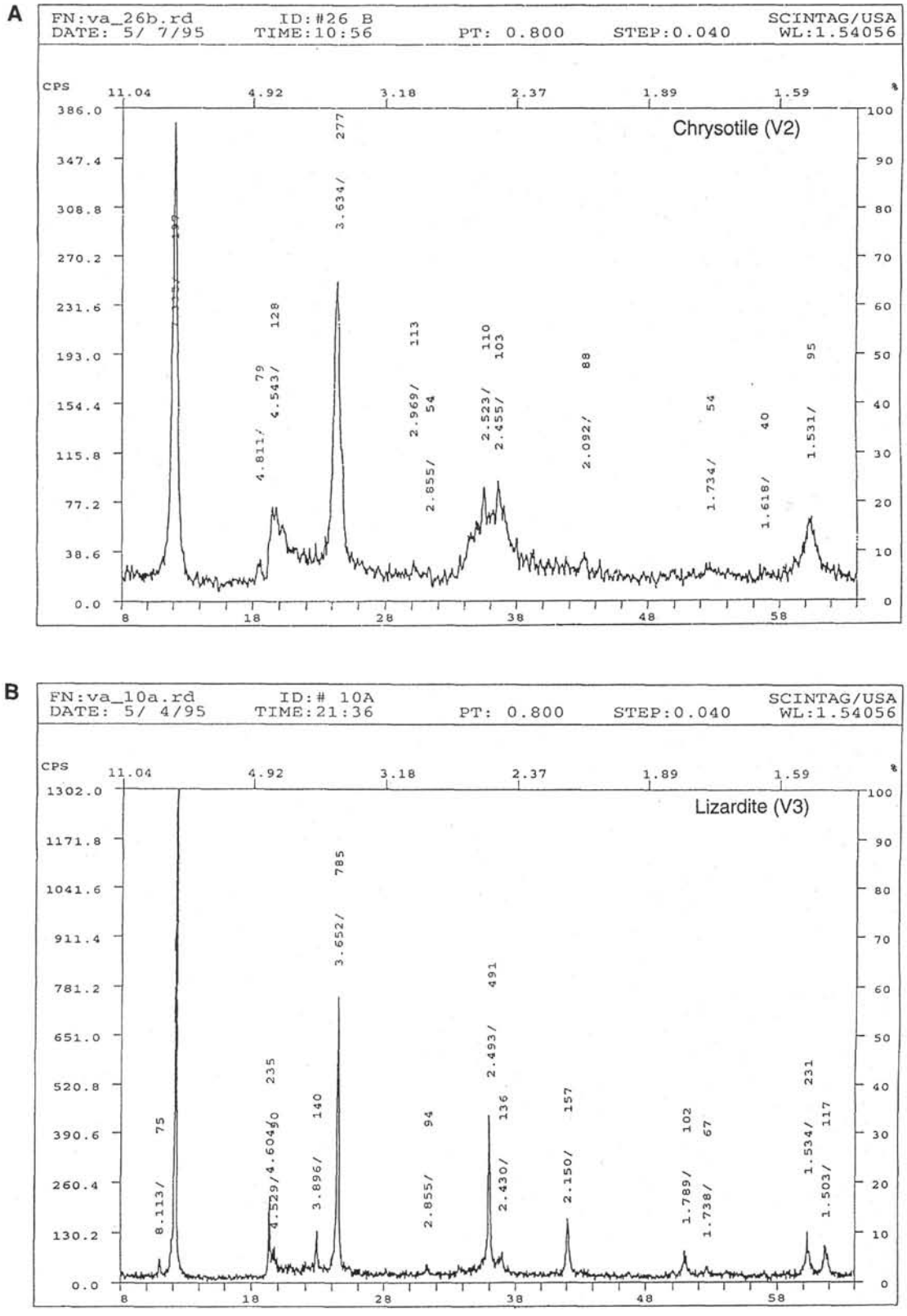

Figure 10. X-ray diffraction patterns of vein material in representative hydrothermal veins in the serpentinized peridotites from Site 920. **A.** Chrysotile in a wispy, irregular V2 vein (Sample 153-920B-9R-2, 111–115 cm). Strong peaks at 2.523, 2.455, 2.092, 1.734, and 1.53 are all representative of chrysotile, corresponding well with the fibrous structure seen on the scanning electron microscope (SEM) photograph in Figure 11A. **B.** Lizardite in a pale green-white, massive V3 vein (Sample 153-920D-22R-5, 65–69 cm). Strong 2.493 and 2.150 peaks suggest that this vein material is made largely of lizardite; there are few other peaks around 2.493, indicating that there may be little (if any) chrysotile in the sample. This interpretation correlates well with the SEM photograph in Figure 11B, which shows flat, tabular plates characteristic of the lizardite structure.

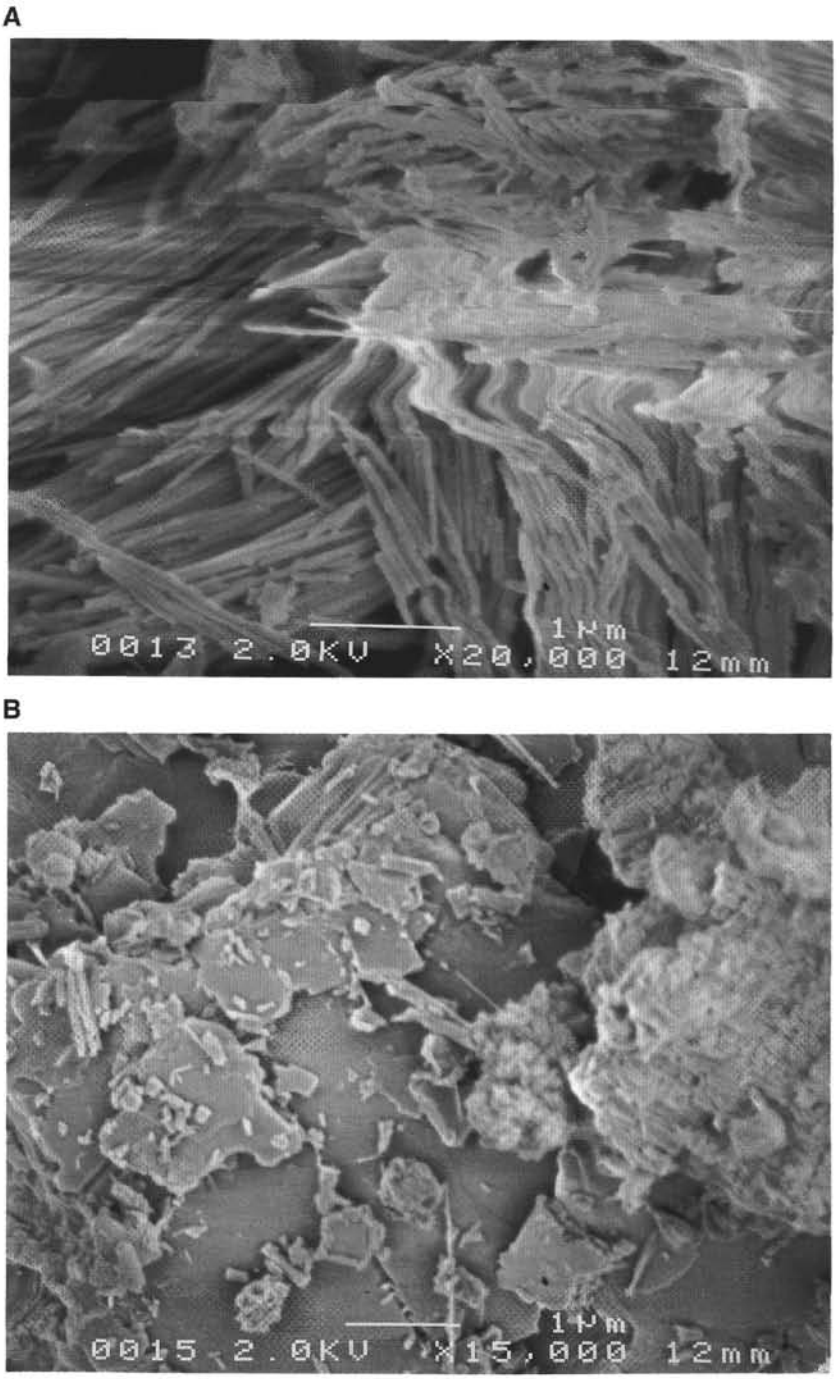

Figure 11. SEM photographs of vein material from (**A**) a fibrous chrysotile V2 vein and (**B**) a massive V3 serpentine vein. Sample numbers correspond to those in Figures 10A and 10B, respectively.

are characterized by faults with relatively steep dips (40°–70°) cutting a more pervasive, gently east-dipping (20°–40°) schistosity, which is possibly related to earlier, low-angle faults and shear zones (Karson, et al., 1987; Mével et al., 1991; Shipboard Scientific Party, 1995). These earlier low-angle faults are interpreted to have normal sense of shearing accompanied by dilation that might have promoted the development of early (V1) extensional veins with oblique slip-fibers. These veins have north-northwest strikes subparallel to the extensional low-angle normal faults.

Exhumation and unroofing of the serpentinized peridotites via continued faulting may have generated lower deviatoric stress with increased fluid pressure. The growth of pure extensional fibrous chrysotile veins (V2) indicates that pore fluid pressures were elevated, allowing expansion as the effective confining pressure was close to zero: $(\sigma_1-\sigma_{2)} \approx 0$. This is consistent with the preferential development of extensional veins subparallel to the preexisting anisotropy defined by the anastomosing serpentine fabric overprinting the mesoscopic porphyroclastic fabric, and is reflected in the strong correspondence of the orientations of the mesoscopic porphyroclastic fabric, anastomosing foliation, and V2 veins (Figs. 16, 17). The changes in the orientations of the V2 veins may reflect change in the local stress field during their development.

Table 4. Composition of different vein generations in serpentinized peridotites from Hole 920B.

Analysis:	1	2	3	4	5	6	7	8	9	10
Texture:	V1 (oblique fiber vein)	V1 (oblique fiber vein)	V1 (oblique fiber vein)	V2 (fibrous extension vein)	V2 (fibrous extension vein)	V2 (fibrous extension vein)	V3 (massive vein)	V3 (massive vein)	V3 (massive vein)	V4 (clay ± pyrite vein)
SiO_2	40.241	41.256	41.682	41.659	42.514	41.609	40.319	41.476	41.634	41.264
TiO_2	0	0	0	0	0	0	0	0	0	0
Al_2O_3	1.185	0.885	0.343	0.822	0.781	0.193	2.551	0.913	0.831	1.8
FeO	4.547	4.915	5.761	2.679	2.805	2.311	2.076	2.51	2.575	3.064
MnO	0.16	0.185	0.196	0.089	0.073	0.051	0.02	0.044	0.062	0.023
MgO	36.034	37.018	36.473	39.556	39.36	40.651	40.26	40.156	40.1	38.535
CaO	0	0	0	0	0	0	0	0	0	0
Na_2O	0.049	0.132	0.036	0.082	0.065	0.007	0	0	0.029	0
K_2O	0	0	0	0	0	0	0	0	0	0
Total	82.22	84.39	84.49	84.89	85.6	84.82	85.23	85.10	85.23	84.69
Si	4.016	4.021	4.071	3.991	4.034	3.986	3.842	3.962	3.972	3.964
Ti	0	0	0	0	0	0	0	0	0	0
Al	0.139	0.102	0.04	0.093	0.087	0.022	0.287	0.103	0.093	0.204
Fe	0.380	0.401	0.471	0.215	0.223	0.185	0.166	0.200	0.205	0.246
Mn	0.013	0.015	0.016	0.007	0.006	0.004	0.002	0.004	0.005	0.002
Mg	5.361	5.378	5.309	5.649	5.567	5.805	5.719	5.717	5.702	5.518
Ca	0	0	0	0	0	0	0	0	0	0
Na	0.01	0.025	0.007	0.015	0.012	0.001	0	0	0.005	0
K	0	0	0	0	0	0	0	0	0	0

Notes: All formulas are calculated on the basis of 14 oxygens. Analyses 1, 2, 8, and 9 are from Sample 153-920B-5R-1, 58–62 cm. Analysis 3 is from Sample 153-920B-5R-2, 67–71 cm. Analyses 4, 5, 7, and 8 are from Sample 153-920B-1W-1, 48–52 cm. Analysis 6 is from Sample 153-920B-12R-2, 143–147 cm. Analysis 10 is from Sample 153-920B-1W-1, 48–52 cm.

The V3 crack-seal veins reflect incremental and successive opening of cracks and vein walls resulting form further stress release and increased pore fluid pressures contemporaneous with unroofing of the serpentinized peridotites. Because both the massive (V3) and fibrous (V2) veins have similar chemical compositions, chemistry alone may not control the differences in their internal fabric. Moody (1976a) suggested that once hydration begins, temperature and pressure only control the speed of the reaction and do not determine whether lizardite or chrysotile form. Development of lizardite (massive) serpentine veining, instead of chrysotile (fibrous), in the latest stages of the hydrothermal alteration may therefore be related to differences in the nature of circulating fluids. This stage might have been associated with the development and operation of steeply east dipping, late normal faults (Karson et al., 1987; Karson and Dick, 1983; Karson, 1990). The majority of V3 veins have consistently steep dips in both Holes 920B and 920D, mimicking the geometry of the observed late normal faults in the MARK area.

V4 veins containing carbonate mineral + pyrite ± clay minerals mark the sealing of extensional fractures by these minerals that were precipitated from very low temperature fluids. Development of these veins might have been associated with emplacement of the exhumed serpentinized peridotites along the rift valley walls and may indicate the general cessation of fluid flow in the ultramafic suite.

Serpentine Diapirism Vs. Tectonic Extension

Serpentine diapirism was invoked originally to explain the occurrence of serpentinites of presumably upper mantle origin in samples dredged from the seafloor along fracture zones (e.g., Miyashiro et al., 1969; Bonatti and Honnorez, 1976; Rona et al., 1987), serpentinized peridotites recovered from Hole 670A in the MARK area (Hébert et al., 1990), and in ophiolites where serpentinites were clearly shown to have been exposed on the seafloor (Abbate et al., 1980). As serpentinized peridotite is less dense than the mafic rocks presumed to lie above, it was assumed that serpentinized ultramafic rocks from the base of the crust would be sufficiently buoyant to intrude diapirically along fracture zones to the near surface. However, dredged serpentine samples provided no clear evidence of diapiric flow. Phipps and Ballotti (1992) tested the rheology of serpentine muds from Mariana forearc seamounts. Serpentinites drilled from these seamounts consist of blocks of massive serpentinite, basaltic igneous rocks, and rare sedimentary and meta-igneous rocks within a sheared serpentinite mud. Strength measurements indicate that the serpentine mud is weak and therefore capable of flow, providing evidence for true serpentine diapirism in the Mariana forearc. Massive serpentinites, however, have been found to have strengths similar to those of granite (Raleigh and Paterson, 1965). For true diapirism to take place, the serpentine must be confined beneath higher density rocks and have low strength. There is no evidence of a serpentine mud matrix associated with the massive serpentinites in this study. Serpentine diapirs would result in extremely large strains that would result in random structures, destruction of the original magmatic structure, and widespread pervasive deformation, several lines of evidence for serpentinite diapirism that are not supported by our observations of the microstructures in the studied serpentinites from Site 920. Hébert et al. (1990) argued that the Site 670 serpentinized peridotite body represents a diapiric intrusion of upper mantle rocks. They suggested that the flat foliation in serpentinized peridotites is a result of a diapiric upward motion of serpentinites during which progressive reequilibration of metamorphic mineral assemblages occurred with further cooling. The flat foliation in the Site 670 serpentinites is analogous to the anastomosing foliation observed in serpentinized peridotites from Site 920, however, and does not present a compelling evidence for serpentinite diapirism at Site 670. Furthermore, serpentinites crop out preferentially along inside corners flanks, where the crust is thin and not compensated isostatically as the gravity studies indicate (i.e., Shaw, 1992; Tucholke and Lin, 1994; Escartin and Lin, 1995). Instead, diapirism should be driven by low-density materials ascending through higher density materials, resulting in a relative gravity low that might be interpreted as thick crust. Therefore, diapiric ascent of serpentinite at Sites 670 and 920 is considered to be extremely unlikely. Exhumation by tectonic extension in the absence of an active magma chamber is a far more likely mechanism for the exposure of serpentinized peridotites on the seafloor in the MARK area.

Sulfide Mineralization in Serpentinized Peridotites

Macroscopic, pyrite-bearing veins are recognized throughout Holes 920B and 920D (Shipboard Scientific Party, 1995; this study), and acicular opaque minerals containing Fe-Ni sulfides that are associated with mesh-textured serpentine were identified in 28 thin sections in this study. Within the recrystallized areas spatially associated with the first-generation (V1) veins and mesh-textured serpentinite, sparse cubic sulfides are present, indicating that sulfides were mobi-

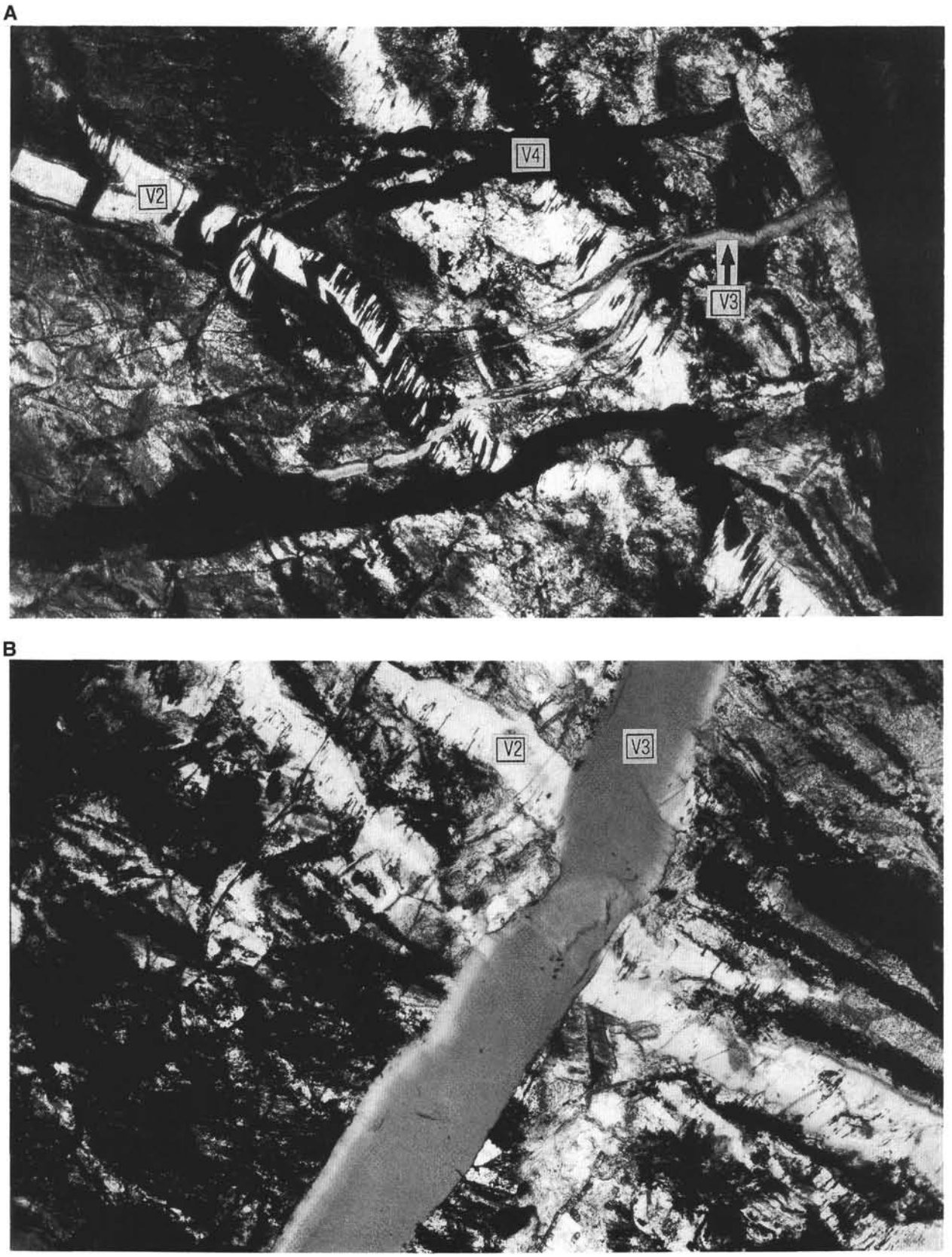

Figure 12. Vein crosscutting relationships. **A.** Fibrous chrysotile vein (V2) is crosscut by wispy, light gray, massive serpentine veins of the V3 generation. Both veins are crosscut by late, opaque, pyrite-bearing veins (V4). Plane-polarized light. Field of view is 3 mm long. Sample 153-920B-1W-1, 91–98 cm. **B.** Massive (gray) serpentine vein (V3) crosscutting fibrous chrysotile vein (V2). Plane-polarized light. Field of view is 3 mm long. Sample 153-920B-1W-1, 91–98 cm.

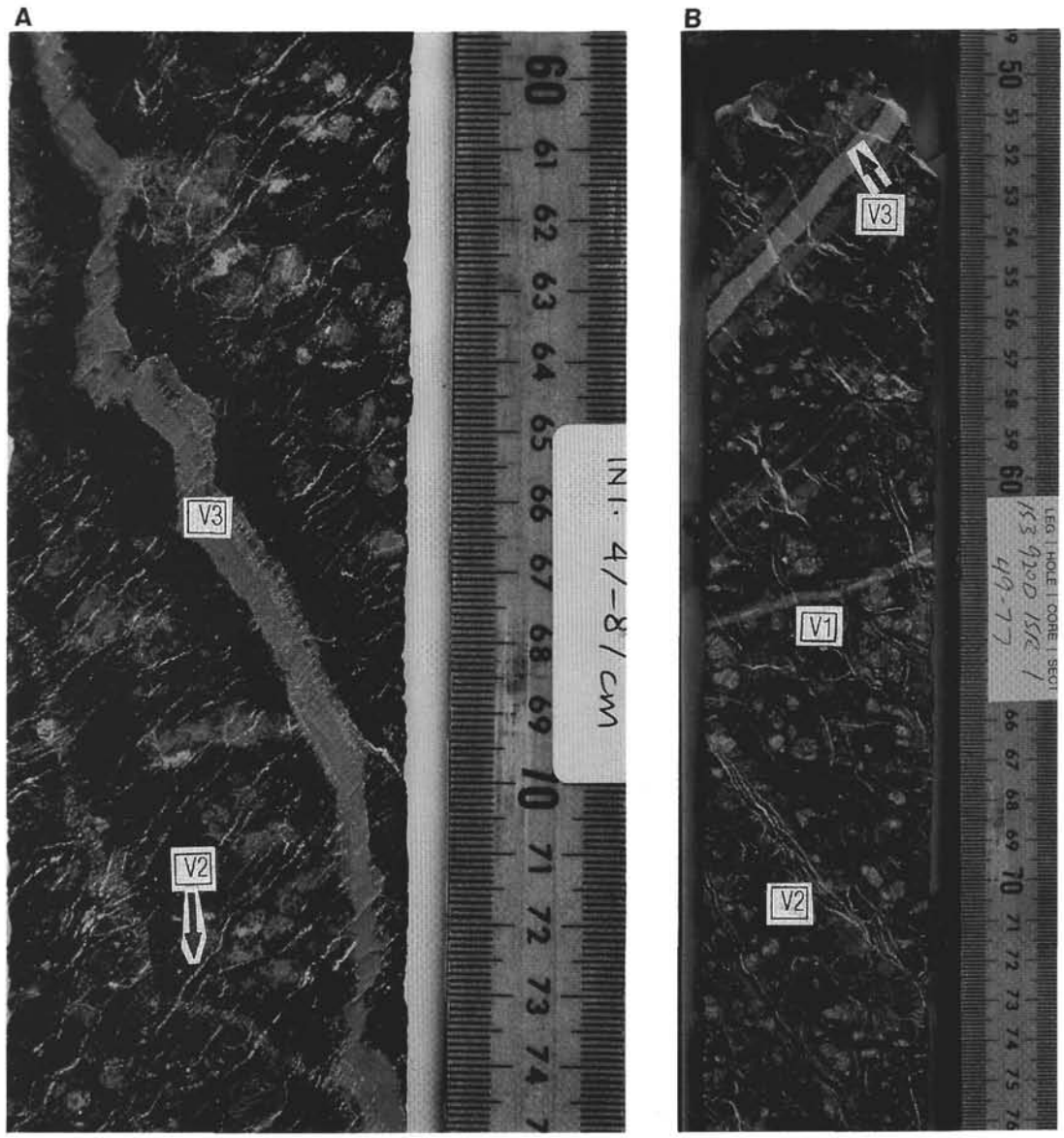

Figure 13. **A.** Discrete irregular serpentine vein (V3) with a dark blue alteration halo. It truncates the wispy white chrysotile veins (V2) at an oblique angle. A narrow stringer of the wallrock material is included near the right wall between 64 and 69 cm (Sample 153-920B-12R-5, 47–87 cm). **B.** Aqua blue, pale green serpentine vein (V3) with a symmetric alteration halo between 50 and 57 cm. The vein is truncated by and slightly offset along subparallel arrays of wispy massive serpentine veins of the same generation (V3). A chlorite + serpentine vein of the V1 generation occurs between 62 and 64 cm. They are both crosscut by wispy V3 serpentine veins. Sample 153-920D-15R-1, 49–77 cm.

lized on a mm-scale during minor recrystallization. Although macroscopic sulfide veins are more easily recognized in hand specimen, disseminated sulfides within the massive, mesh-textured serpentinite may be far more abundant. Development of Fe-Ni sulfides has previously been documented in serpentinites (e.g., Dick, 1974; Shiga, 1987; Frost, 1985). These studies attributed the stabilization of sulfide minerals, and native metal alloys such as josephinite (Dick, 1974) in serpentinites to the locally reducing conditions present during initial hydration and serpentinization of a peridotite. The association of Fe-Ni sulfide minerals with the serpentine mesh texture supports this argument, as they are clearly associated with the early, pseudomorphic serpentine textures. They do not occur, however, within partially serpentinized peridotites. The most likely source for the sulfur is seawater sulfate, which could have been reduced during the serpentinization process. This phenomenon requires further work on the nature and extent of sulfide mineralization in serpentinized ultramafic rocks, which is beyond the scope of this study. If sulfide-bearing serpentinites are abundant at slow-spreading ridges, as in the MARK area of the Mid-Atlantic Ridge seafloor spreading system, they may act as a significant sink for sulfur and should perhaps be considered in calculations of the sulfur content of oceanic lithosphere, such as those made by Alt (1995) for composite oceanic crust.

ACKNOWLEDGMENTS

This work was supported by a grant from JOI-USSAC to Y.D. The authors thank D. O'Hanley, G. Harper, and Deborah Kelley for helpful discussions on different aspects of serpentinization and hydrothermal alteration of ultramafic rocks. Critical but constructive comments by M. Cannat, G. Früh-Green, G. Hirth, and J. Karson improved the paper.

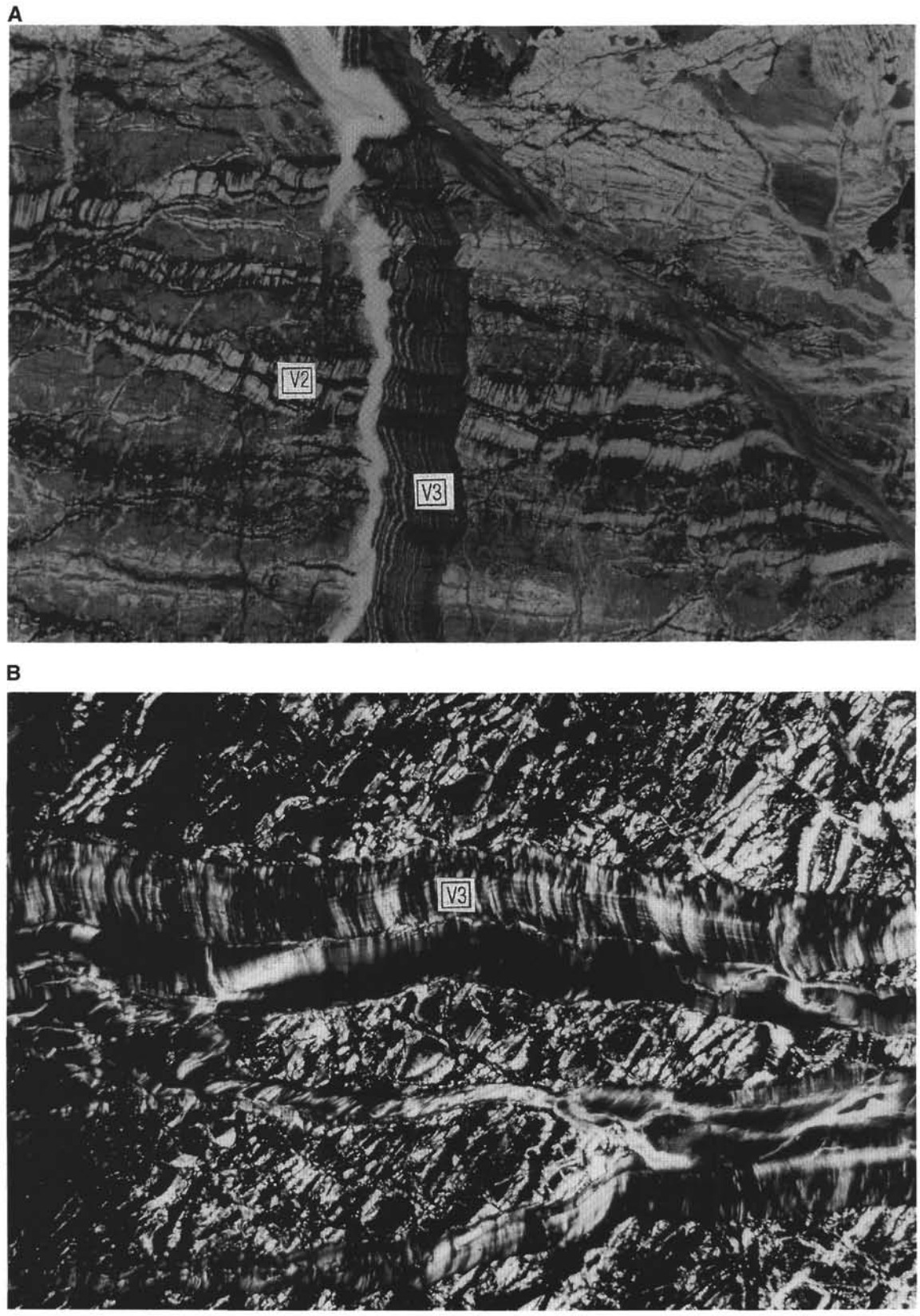

Figure 14. **A.** Vertical serpentine vein (V3) with a banded internal fabric crosscutting the nearly subhorizontal fibrous chrysotile veins of the V2 generation. Wallrock inclusions within and along the bands indicate incremental opening of the vein crack along the walls. Sample 153-920D-5R-1, 90–95 cm. Plane-polarized light. Field of view is 3 mm long. **B.** Branching serpentine (lizardite) veins of the V3 generation with crack-seal bands and pseudo-fibrous internal fabric. Sample 153-920B-1W-1, 91–98 cm. Crossed polars. Field of view is 3 mm long.

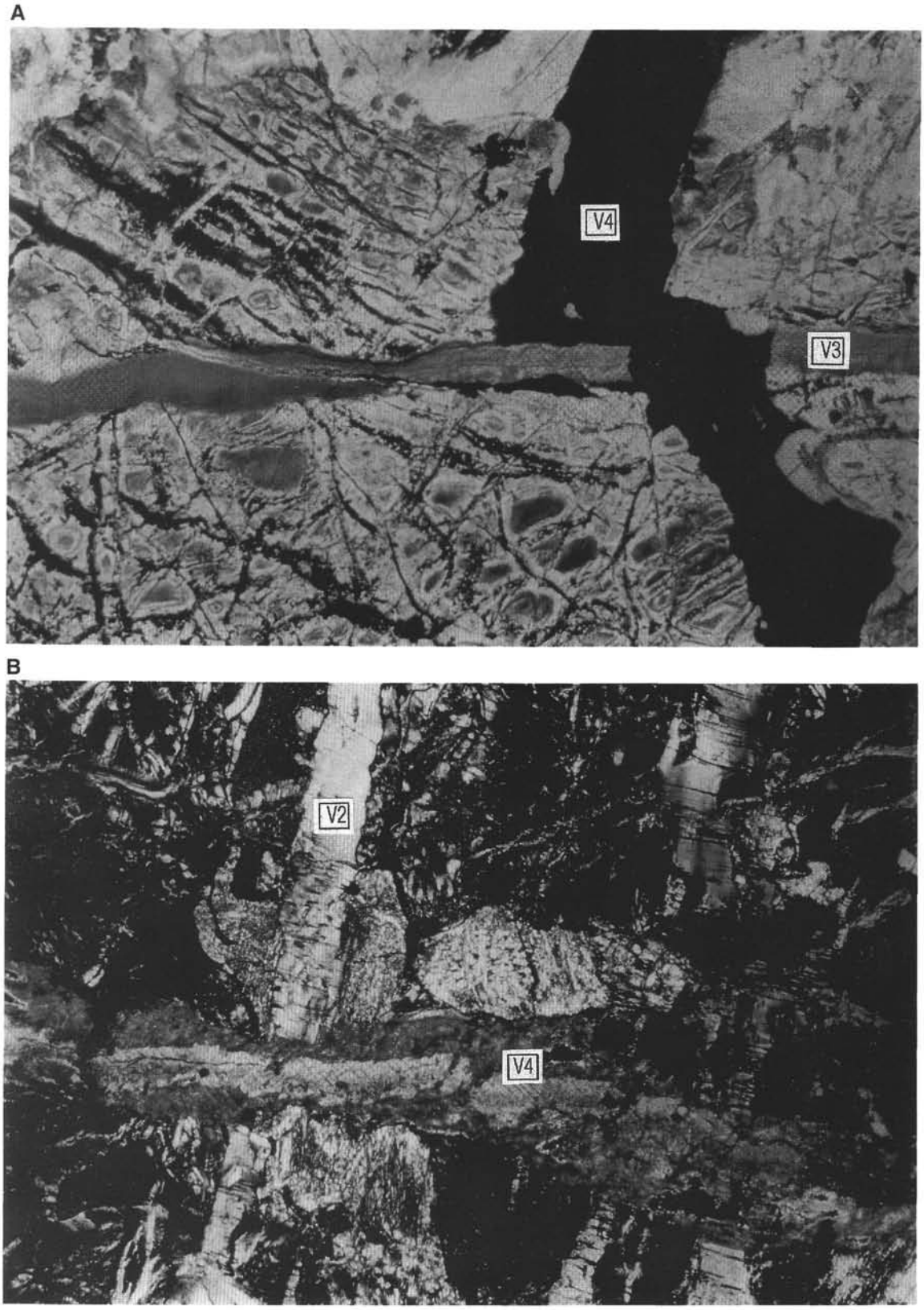

Figure 15. **A.** V4 vein, containing pyrite + hematite + clay, crosscuts the mesh-textured serpentine and a banded V3 vein. This V4 vein is partially developed along the older V3 vein reactivating it. Sample 153-920B-1W-1, 48–52 cm. Plane-polarized light. Field of view is 3 mm. **B.** V4 vein, containing carbonate + clay ± serpentine, crosscuts several subparallel fibrous chrysotile veins of V2 generation. Carbonate mineral is in the center of the vein and represents a later stage of filling than the clay + serpentine filling along the vein walls. Sample 153-920B-9R-2, 43–49 cm. Crossed polars. Field of view is 1 mm.

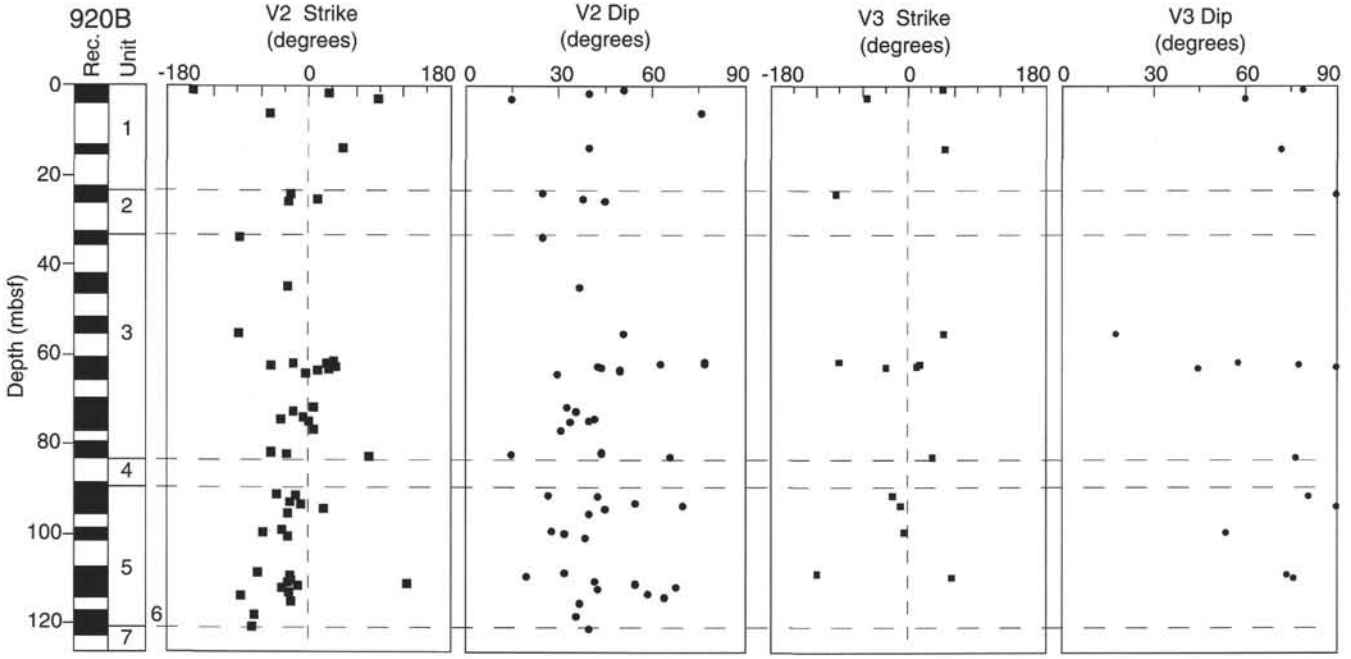

Figure 16. Downhole variations in dip and strike angles of V2 and V3 vein generations in Hole 920B. Rec = core recovery (black bars)

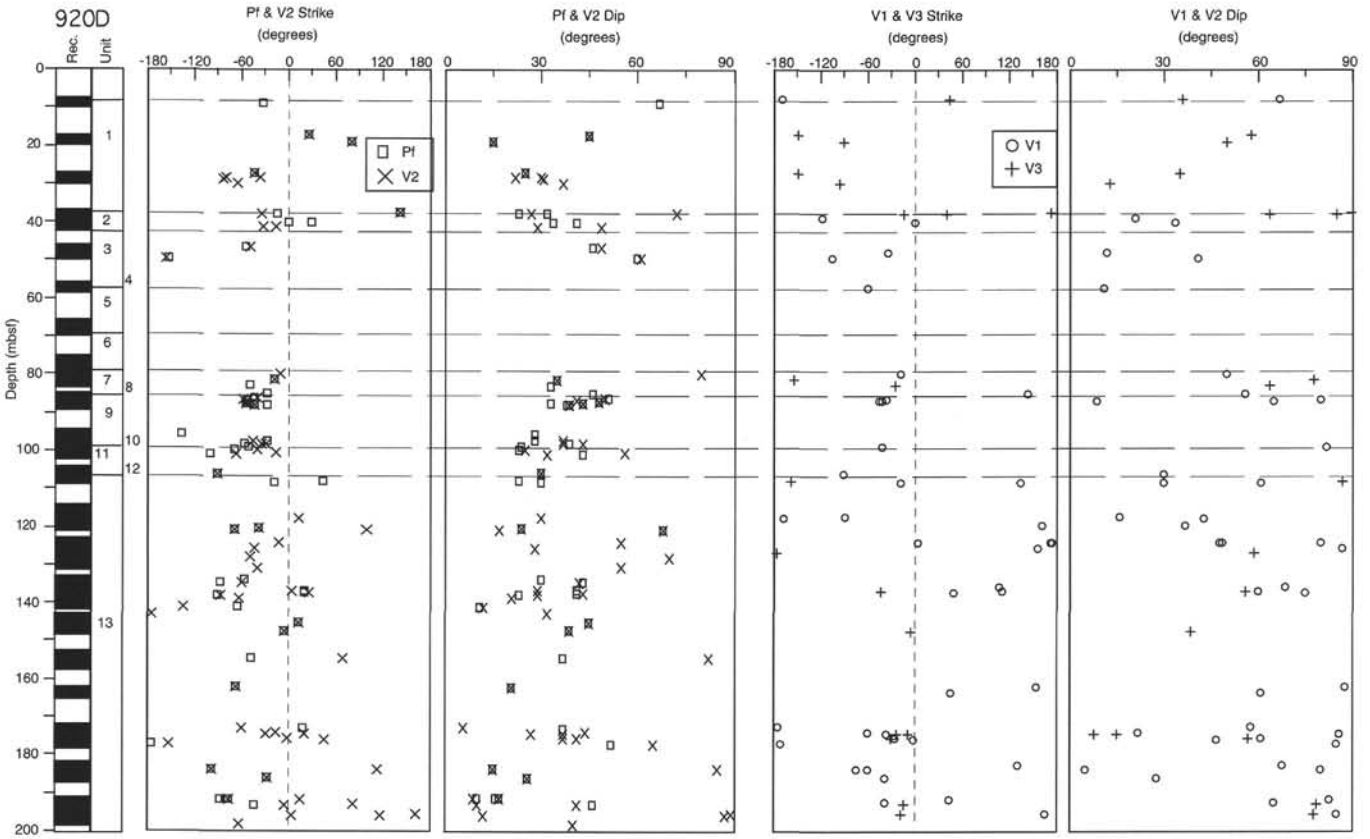

Figure 17. Downhole variations in dip and strike angles of the mesoscopic porphyroclastic fabric (Pf) and V1, V2, and V3 vein generations in Hole 920D. Rec = core recovery (black bars).

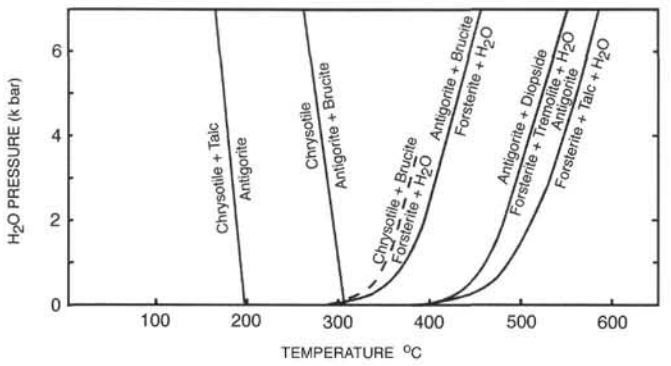

Figure 18. Temperature-P_{H2O} diagram for reactions in the system CaO-MgO-Al_2O_3-SiO_2-H_2O involving the composition Mg_2SiO_4. Modified from Evans (1977) and Evans et al. (1976).

Table 5. Tectonic interpretation of low-temperature deformation and hydrothermal alteration of the upper mantle in the MARK area.

Timing	Cause/event	Effect
Early	Depression of isotherms (in the absence of a magma chamber).	Pervasive bulk-rock serpentinization.
	Brittle cracking down to the upper mantle penetration of seawater along cracks (300°–400°C).	Development of mesh texture.
	Extensional tectonics, low-angle normal faulting accompanied by dilation (<350°C).	Development of extensional V1 veins with oblique fibers.
	Unroofing of serpentinized peridotites (<350°C).	Development of pure-extensional V2 veins.
	Increased fluid pressure, lower deviatoric stress.	
	Block faulting.	
	Continued unroofing of the serpentinized peridotites (<350°C).	Development of V3 crack-seal veins.
	Incremental opening resulting from stress release.	
Late	Diminished fluid flow on the shoulders of the rift valley.	Sealing of extensional fractures by carbonate mineral + pyrite and carbonate mineral + clay veins (V4).

REFERENCES

Abbate, E., Bortolotti, V., and Principi, G., 1980. Apennine ophiolites: a peculiar oceanic crust. *Ofioliti,* 1:59–96.

Alt, J.C., 1995. Sulfur isotopic profile through the oceanic crust: sulfur mobility and seawater-crustal sulfur exchange during hydrothermal alteration. *Geology,* 23:585–588.

Bonatti, E., and Honnorez, J., 1976. Sections of the earth's crust in equatorial Atlantic. *J. Geophys. Res.,* 81:4104–4116.

Brown, J.R., and Karson, J.A., 1988. Variations in axial processes on the Mid-Atlantic Ridge: the median valley of the MARK area. *Mar. Geophys. Res.,* 10:109–138.

Cannat, M., 1993. Emplacement of mantle rocks in the seafloor at mid-ocean ridges. *J. Geophys. Res.,* 98:4163–4172.

Cannat, M., Bideau, D., and Bougault, H., 1992. Serpentinized peridotites and gabbros in the Mid-Atlantic Ridge axial valley at 15°37′N and 16°52′N. *Earth Planet. Sci. Lett.,* 109:87–106.

Cannat, M., Juteau, T., and Berger, E., 1990. Petrostructural analysis of the Leg 109 serpentinized peridotites. *In* Detrick, R., Honnorez, J., Bryan, W.B., Juteau, T., et al., *Proc. ODP, Sci. Results,* 106/109: College Station, TX (Ocean Drilling Program), 47–57.

Cannat, M., Karson, J.A., Miller, D.J., et al., 1995. *Proc. ODP, Init. Repts.,* 153: College Station, TX (Ocean Drilling Program).

Cannat, M., Mével, C., Maia, M., Deplus, C., Durand, C., Gente, P., Agrinier, P., Belarouchi, A., Dubuisson, G., et al., 1995. Thin crust, ultramafic exposures, and rugged faulting patterns at the Mid-Atlantic Ridge (22°–24°N). *Geology,* 23:49–52.

Caruso, L.J., and Chernosky, J.V., Jr., 1979. The stability of lizardite. *Can. Mineral.,* 17:757–769.

Chernosky, J.V., Jr., 1973. An experimental investigation of the serpentine and chlorite group minerals in the multisystem MgO-Al_2O_3-SiO_2-H_2O. [Ph.D. thesis]. Mass. Inst. Tech., Cambridge, MA.

Chernosky, J.V., Jr., Berman, R.G., and Bryndzia, L.T., 1988. Serpentine and chlorite equilibria. *In* Bailey, S.W. (Ed.), *Hydrous Phyllosilicates Other than Micas.* Rev. Mineral., 19:295–346.

Detrick, R.S., Mutter, J.C., Buhl, P., and Kim, I.I., 1990. No evidence from multichannel seismic reflection data for a crustal magma chamber in the MARK area on the Mid-Atlantic Ridge. *Nature,* 347:61–64.

Dick, H.J.B., 1974. Terrestrial nickel-iron from the Josephine peridotite, its geologic occurrence, associations and origin. *Earth Planet. Sci. Lett.,* 24:291–298.

Escartin, J., and Lin, J., 1995. Ridge offsets, normal faulting, and gravity anomalies of slow spreading ridges. *J. Geophys. Res.,* 100:6163–6177.

Evans, B.W., 1977. Metamorphism of alpine peridotite and serpentinite. *Annu. Rev. Earth Planet. Sci.,* 5:398–447.

Evans, B.W., Johannes, W., Oterdoom, H., and Trommsdorff, V., 1976. Stability of chrysotile and antigorite in the serpentine multisystem. *Schweiz. Mineral. Petrogr. Mitt.,* 56:79–93.

Frost, B.R., 1985. On the stability of sulfides, oxides, and native metals in serpentine. *J. Petrol.,* 26:31–63.

Hébert, R., Adamson, A.C., and Komor, S.C., 1990. Metamorphic petrology of ODP Leg 109, Hole 670A serpentinized peridotites: serpentinization processes at a slow spreading ridge environment. *In* Detrick, R., Honnorez, J., Bryan, W.B., Juteau, T., et al., *Proc. ODP, Sci. Results,* 106/109: College Station, TX (Ocean Drilling Program), 103–115.

Johannes, W., 1968. Experimental investigation of the reaction forsterite + H_2O = serpentine + brucite. *Contrib. Mineral. Petrol.,* 19:309–315.

Juteau, T., Berger, E., and Cannat, M., 1990. Serpentinized, residual mantle peridotites from the M.A.R. median valley, ODP Hole 670A (21°10′N, 45°02′W, Leg 109): primary mineralogy and geothermometry. *In* Detrick, R., Honnorez, J., Bryan, W.B., Juteau, T., et al., *Proc. ODP, Sci. Results,* 106/109: College Station, TX (Ocean Drilling Program), 27–45.

Karson, J.A., 1990. Seafloor spreading on the Mid-Atlantic Ridge: implications for the structure of ophiolites and oceanic lithosphere produced in slow-spreading environments. *In* Malpas, J., Moores, E.M., Panayiotou, A., and Xenophontos, C. (Eds.), *Ophiolites: Oceanic Crustal Analogues:* Proc. Symp. "Troodos 1987": Nicosia, Cyprus (Minist. Agric. Nat. Resour.), 547–555.

Karson, J.A., and Dick, H.J.B., 1983. Tectonics of ridge-transform intersections at the Kane Fracture Zone. *Mar. Geophys. Res.,* 6:51–98.

Karson, J.A., Thompson, G., Humphris, S.E., Edmond, J.M., Bryan, W.B., Brown, J.R., Winters, A.T., Pockalny, R.A., Casey, J.F., Campbell, A.C., Klinkhammer, G., Palmer, M.R., Kinzler, R.J., and Sulanowska, M.M., 1987. Along-axis variations in seafloor spreading in the MARK area. *Nature,* 328:681–685.

Kirby, S.H., 1983. Rheology of the lithosphere. *Rev. Geophys.,* 21:1458–1487.

Kunze, G., 1958. Die gewellte Strukture des Antigorites, II. *Zeit. Krist.,* 110:282–320.

Mével, C., Cannat, M., Gente, P., Marion, E., Auzende, J.-M., and Karson, J.A., 1991. Emplacement of deep crustal and mantle rocks on the west median valley wall of the MARK area (MAR 23°N). *Tectonophysics,* 190:31–53.

Michael, P.J., and Bonatti, E., 1985. Peridotite composition from the North Atlantic: regional and tectonic variations and implications for partial melting. *Earth Planet. Sci. Lett.,* 73:91–104.

Miyashiro, A., Shido, F., and Ewing, M., 1969. Composition and origin of serpentinites from the Mid-Atlantic Ridge, 24° and 30°N latitude. *Contrib. Mineral. Petrol.,* 23:117–127.

Moody, J.B., 1976a. Sepentinization: a review. *Lithos,* 9:125–138.

———, 1976b. An experimental study on the serpentinization of iron-bearing olivines. *Can. Mineral.,* 14:462–478.

O'Hanley, D.S., 1991. Fault-related phenomena associated with hydration and serpentine recrystallization during serpentinization. *Can. Mineral.,* 29:21–35.

O'Hanley, D.S., Chernosky, J.V., Jr., and Wicks, F.J., 1989. The stability of lizardite and chrysotile. *Can. Mineral.,* 27:483–493.

Phipps, S.P., and Ballotti, D., 1992. Rheology of serpentinite muds in the Mariana-Izu-Bonin forearc. *In* Fryer, P., Pearce, J.A., Stokking, L.B., et al., *Proc. ODP, Sci. Results,* 125: College Station, TX (Ocean Drilling Program), 363–372.

Purdy, G.M., and Detrick, R.S., 1986. Crustal structure of the Mid-Atlantic Ridge at 23°N from seismic refraction studies. *J. Geophys. Res.,* 93:3739–3762.

Raleigh, C.B., and Paterson, M.S., 1965. Experimental deformation of serpentinite and its tectonic implications. *J. Geophys. Res.,* 70:3965–3985.

Ramsay, J.G., 1980. The crack-seal mechanism of rock deformation. *Nature,* 284:135–139.

Ramsay, J.G., and Huber, M.I., 1983. *The Techniques of Modern Structural Geology* (Vol. 1): *Strain Analysis:* London (Acad. Press).

Rona, P.A., Widenfalk, L., and Boström, K., 1987. Serpentinized ultramafics and hydrothermal activity at the Mid-Atlantic Ridge crest near 15°N. *J. Geophys. Res.,* 92:1417–1427.

Sanford, R.F., 1981. Mineralogical and chemical effects of hydration reactions and applications to serpentinization. *Am. Mineral.,* 66:290–297.

Scambelluri, M., Müntener, O., Hermann, J., Piccardo, G., and Tommsdorff, V., 1995. Subduction of water into the mantle: history of an Alpine peridotite. *Geology,* 23:459–462.

Shaw, P.R., 1992. Ridge segmentation, faulting and crustal thickness in the Atlantic Ocean. *Nature,* 358:490–492.

Shiga, Y., 1987. Behavior of iron, nickel, cobalt and sulfur during serpentinization, with reference to the hyachine ultramafic rocks of the Kamaishi mining district, northeastern Japan. *Can. Mineral.,* 25:611–624.

Shipboard Scientific Party, 1995. Site 920. *In* Cannat, M., Karson, J.A., Miller, D.J., et al., *Proc. ODP, Init. Repts.,* 153: College Station, TX (Ocean Drilling Program), 45–119.

Spear, F.S., 1981. An experimental study of hornblende stability and compositional variability in amphibolite. *Am. J. Sci.,* 281:697–734.

Stakes, D., Mével, C., Cannat, M., and Chaput, T., 1991. Metamorphic stratigraphy of Hole 735B. *In* Von Herzen, R.P., Robinson, P.T., et al., *Proc. ODP, Sci. Results,* 118: College Station, TX (Ocean Drilling Program), 153–180.

Tucholke, B.E., and Lin, J., 1994. A geological model for the structure of ridge segments in slow-spreading ocean crust. *J. Geophys. Res.,* 99:11937–11958.

Ulmer, P., and Trommsdorff, V., 1995. Serpentine stability to mantle depths and subduction related magmatism. *Science,* 268:858–861.

Vanko, D.A., and Stakes, D.S., 1991. Fluids in oceanic layer 3: evidence from veined rocks, Hole 735B, Southwest Indian Ridge. *In* Von Herzen, R.P., Robinson, P.T., et al., *Proc. ODP, Sci. Results,* 118: College Station, TX (Ocean Drilling Program), 181–215.

Wegner, W.W., and Ernst, W.G., 1983. Experimentally determined hydration and dehydration rates in the system $MgO\text{-}SiO_2\text{-}H_2O$. *Am. J. Sci.,* 283:151–180.

Wenner, D.B., and Taylor, H.P., Jr., 1971. Temperatures of serpentinization of ultramafic rocks based on $^{16}O/^{18}O$ fractionation between coexisting serpentine and magnetite. *Contrib. Mineral. Petrol.,* 32:165–185.

Wicks, F.J., and O'Hanley, D.S., 1988. Serpentine minerals: structure and petrology. *In* Bailey, S.W. (Ed.), *Hydrous Phyllosilicates.* Rev. Mineral., 19:91–101.

Wicks, F.J., and Whittaker, E.J.W., 1977. Serpentine textures and serpentinization. *Can. Mineral.,* 15:459–488.

Wicks, F. J., and Zussman, J., 1975. Microbeam X-ray diffraction patterns of the serpentine minerals. *Can. Mineral.,* 13:244–258.

Date of initial receipt: 7 August 1995
Date of acceptance: 23 April 1996
Ms 153SR-004